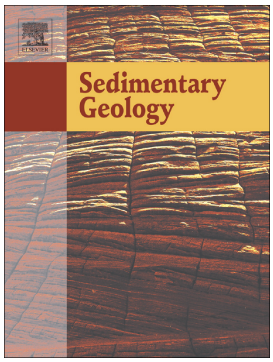

Reduced sediment supply in a fast eroding landscape? A multi-proxy sediment budget of the upper Rhône basin, Central Alps

Laura Stutenbecker, Romain Delunel, Fritz Schlunegger, Tiago Adrião Silva, Branimir Šegvić, Stéphanie Girardclos, Maarten Bakker, Anna Costa, Stuart N. Lane, Jean-Luc Loizeau, Peter Molnar, Naki Akçar, Marcus Christl

PII: S0037-0738(17)30289-0
DOI: https://doi.org/10.1016/j.sedgeo.2017.12.013
Reference: SEDGEO 5285

To appear in:

Received date: 3 May 2017
Revised date: 11 December 2017
Accepted date: 14 December 2017

Please cite this article as: Laura Stutenbecker, Romain Delunel, Fritz Schlunegger, Tiago Adrião Silva, Branimir Šegvić, Stéphanie Girardclos, Maarten Bakker, Anna Costa, Stuart N. Lane, Jean-Luc Loizeau, Peter Molnar, Naki Akçar, Marcus Christl , Reduced sediment supply in a fast eroding landscape? A multi-proxy sediment budget of the upper Rhône basin, Central Alps. The address for the corresponding author was captured as affiliation for all authors. Please check if appropriate. Sedgeo(2017), https://doi.org/10.1016/j.sedgeo.2017.12.013

Reduced sediment supply in a fast eroding landscape? A multi-proxy sediment budget of the upper Rhône basin, Central Alps

Laura Stutenbecker[1]*, Romain Delunel[1], Fritz Schlunegger[1], Tiago Adrião Silva[2,3], Branimir Šegvić[3,8], Stéphanie Girardclos[3,4], Maarten Bakker[5], Anna Costa[6], Stuart N. Lane[5], Jean-Luc Loizeau[2], Peter Molnar[6], Naki Akçar[1], Marcus Christl[7]

[1] Institute of Geological Sciences, University of Bern, Baltzerstrasse 1+3, 3012 Bern, Switzerland

[2] Department F.-A. Forel for environmental and aquatic sciences, University of Geneva, 1211 Geneva, Switzerland

[3] Department of Earth Sciences, University of Geneva, 1205 Geneva, Switzerland

[4] Institute for Environmental Sciences, University of Geneva, 1205 Geneva, Switzerland

[5] Institute of Earth Surface Dynamics, University of Lausanne, 1015 Lausanne, Switzerland

[6] Institute of Environmental Engineering, ETH Zürich, 8093 Zürich, Switzerland

[7] Laboratory of Ion Beam Physics, ETH Zürich, 8093 Zürich, Switzerland

[8] Department of Geosciences, Texas Tech University, Lubbock, TX 79409, USA

*corresponding author: laura.stutenbecker@geo.unibe.ch

Abstract

Alpine water and sediment supply influence the sediment budget of many important European fluvial systems such as the Rhine, Rhône and Po rivers. In the light of human induced climate change and

landscape modification, it becomes increasingly important to understand the mechanisms of sediment production and supply in Alpine sediment systems. This study aims to investigate the modern sediment budget of the upper Rhône basin, one of the largest Alpine intramontane watersheds, located in the Central Alps of southwestern Switzerland. Major areas of sediment generation are fingerprinted by framework petrography, heavy mineral concentrations and bulk geochemistry. The relative contributions of the three major sources to the sediment of the trunk Rhône river are identified by compositional mixing modelling. Concentrations of the terrestrial cosmogenic nuclide ^{10}Be measured in quartz separated from fluvial sediments provide spatially averaged denudation rates for selected tributary basins. Results from sediment fingerprinting and mixing modelling suggest that tributaries located in the North and the East of the catchment are generating most of the sediment transported by the Rhône river to its primary sedimentary sink in Lake Geneva. Despite having some of the highest denudation rates within the basin, tributaries located in the southern area of the Rhône basin are relatively underrepresented in the sediment budget of the Rhône river. These tributaries are severely affected by human activities, for example through sediment mining as well as water and sediment abstraction in large hydropower reservoirs. Together, these processes reduce the basin-wide sediment discharge by about 50%, thereby explaining most of the observed compositional pattern. In addition, there is evidence suggesting that large amounts of glaciogenic sediments are currently supplied by retreating glaciers. Glaciogenic material with its low ^{10}Be concentrations can lead to a significant

overestimation of denudation rates and thus limit the applicability of cosmogenic nuclide analysis in such glaciated settings.

Keywords

Fingerprinting; Geochemistry; Denudation rates; Cosmogenic nuclides; Sediment generation; Human impact

1. Introduction

The world's river networks are important sedimentary systems that regulate the transport of water and sediment between sources and sinks (Dearing & Jones, 2003; Meybeck, 2003; Vörösmarty et al., 2003; Syvitski & Milliman, 2007; Hinderer et al., 2013). The absolute quantities and rates of sediment supply can considerably influence biogeochemical cycles (e.g. Ludwig & Probst 1996; Stallard 1998), biodiversity (e.g. Snelgrove 1997; McLaughlin et al. 2003) and sediment dynamics (e.g. Goodbred & Kuehl 1999; Diekmann et al. 2008) in relation to sedimentary sinks, as well as general landscape evolution (Tucker & Bras, 1998; Phillips, 2005, Korup, 2009), and even mountain building processes (e.g. Willett 1999; Champagnac et al. 2012). Hence, many studies, from surveys on single river catchments through to the global scale, have analysed the factors that might control sediment dynamics, such as geomorphology and relief, climate and tectonics. As the time scales of interest become shorter, human activities have also been shown to be important (Milliman & Syvitski, 1992; Summerfield & Hulton, 1994; Harrison, 2000; Montgomery & Brandon, 2002, Vörösmarty et al., 2003; Molnar et al., 2007; Hinderer, 2012).

In central Europe, most of the major fluvial systems such as the Rhine, Rhône, Po and Danube rivers, are fed by Alpine headwaters or tributaries. Alpine-derived material has thus been found to be transported out of the orogen for several hundred to thousands of kilometres (Hay et al., 1992; Tebbens et al., 1995; Bernet et al., 2004), demonstrating the importance of the Alpine orogen as a critical sediment source for the European continent. Indeed, high relief, glacial cover, orographic precipitation, active deformation and seismicity together with favourable litho-tectonic architecture have collectively resulted in some of the highest denudation rates currently measured in Europe (Wittmann et al., 2007; Norton et al., 2011; Cruz Nunes et al., 2015). In such complex orogenic systems, external controlling factors, different time scales and sensitive feedback mechanisms considerably complicate the understanding of sediment generation. This is particularly critical over the Anthropocene time scales, in which water and sediment cycles, especially in the Alpine system, are increasingly influenced by rapid climate change (Micheletti & Lane, 2016; Lane et al., 2017) and human activity (Anselmetti et al., 2007; Fatichi et al., 2015).

This progress aside, we still know very little about how spatial variability in intra-basin properties (e.g. relief, geology, geomorphology, climate) interact with human activities to influence sediment transfer from source to sink. Recent and direct impacts of human activity (e.g. hydropower exploitation) on sediment flux in Alpine basins may correlate (whether causally or spuriously) with, for example, the effects of global climate change (Costa et al., 2017). This makes it critical to distinguish “natural” variability in sediment transfer in space and time against which human impacts can be

judged. Thus, this study aims to understand the spatial distribution of sediment sources and the mechanisms of modern sediment generation in the upper Rhône basin, which is a large, rapidly changing intramontane watershed located within the Central Alps in southwestern Switzerland. In order to quantify processes of sediment generation, areas acting as important sediment sources are identified using various fingerprinting techniques and their relative contributions to the Rhône sediment budget is estimated by compositional mixing modelling. Spatially averaged denudation rates inferred from the concentrations of the terrestrial cosmogenic nuclide ^{10}Be provide absolute quantities of sediment production in selected tributary basins.

2. Setting

The upper Rhône river, located in the high Alps of southwestern Switzerland, drains a ca. 5400 km^2 large catchment between the Rhône glacier's snout (2250 m a.s.l.) and Lake Geneva (372 m a.s.l.). The drainage area of the Rhône river can be sub-divided into ca. 50 major (>10 km^2) tributary catchments (Fig. 1). The size and geometry of these tributary basins vary significantly within the Rhône basin, with the largest and longest tributary basins being located south of the Rhône river.

The watershed of the Rhône river can be considered as a closed intramontane basin with the primary sedimentary sink being located in Lake Geneva (Fig. 1). The upper Rhône basin is one of the largest inner-orogen watersheds in the European Alps with some of the highest mountain peaks, highest relief, largest glaciers and the

highest rock uplift (>1.5 mm/yr) and highest measured denudation rates at present (Schlatter et al., 2005; Wittmann et al., 2007; Schlunegger et al., 2009; Norton et al., 2011). Accordingly, sediment production and supply is driven mainly by glacial erosion and mass wasting processes on steep hillslopes, which are largely controlled by precipitation, snow and ice melt (Costa et al., 2017). The mean annual precipitation in the upper Rhône basin amounts to about 1400 mm/yr with a strong spatial variability driven by an orographic effect (Costa et al., 2017). Today, the mean annual water discharge measured at the basin outlet is about 180 m^3/s, and peaks with the maximum of the snow and ice melt in the summer months (Costa et al., 2017). The Rhône valley contained some of the thickest alpine glaciers throughout the Quaternary period (Florineth & Schlüchter 1998; Bini et al. 2009), and today hosts some of the largest Alpine glaciers (e.g. the Aletsch glacier) (Joerin et al., 2006). Recent glacial cover in the Rhône valley is 14%, with individual watersheds in the Northeast and Southeast being glaciated up to 50%. Geodetic levelling surveys suggest a spatial gradient of recent rock uplift rates with a maximum of ca. 1.5 mm/yr in the Northeast to a minimum of 0.3 mm/yr in the West of the catchment (Schlatter et al., 2005).

Within the last century, the Rhône basin became increasingly influenced by anthropogenic impact. The main Rhône river was channelized twice in the periods of 1863 – 1894 and 1930 – 1960, which reduced the length of the river from 414 to 251 km (Weber et al., 2007; Meile et al., 2011). This dramatically decreased the fish diversity in the Rhône, with only 2 out of 18 historically reported fish species having been found in 2007 (Weber et al., 2007). Sediment is extracted along large floodplains within the Rhône river, and also

within the tributary streams (Fig. 1). Hydropower dams were constructed since the beginning of the 20th century with a main construction phase between 1957 and 1974 (Loizeau & Dominik, 2000). Today, the total capacity of storage reservoirs connected to the ca. 40 hydropower dams located in the area exceeds 1.35 km^3, which amounts to about 20% of the average annual water discharge of the Rhône River (Loizeau & Dominik, 2000).

The study area comprises basically three litho-tectonic units with different geological histories (Schmid et al., 1996; 2004). The Central Alps were formed by the collision of the southern European continental margin with the Adria microplate, thereby closing two ocean basins located in between them, i.e. the Valais trough and the Piedmont-Liguria ocean (Trümpy, 1960; Schmid et al., 2004). Remnants of both basins, as well as the microcontinent Briançonnais, which separated both basins, are today incorporated in the Alpine orogen and referred to as the Penninic domain (Schmid et al., 2004). In terms of lithologies, the Penninic domain comprises ophiolites of the Valais and Piedmont-Liguria oceans (metabasalts, metagabbros, serpentinites, calcschists, flysch sediments) as well as gneisses and micashists from the Briançonnais continent. The European units comprise autochthonous slices of crystalline basement (External massifs, Herwegh et al., 2017) as well as "sub-penninic" (i.e. allochthonous) basement nappes such as the Gotthard nappe and the Lepontine dome, which contain mostly metagranites and gneisses. The folded sedimentary cover of the European basement units, the Helvetic nappes (Fig. 1), comprises mostly carbonates from a passive margin setting. Rocks of Adria provenance are only present in the Dent Blanche complex in the South of the study area (Fig. 1), where

they are represented exclusively by high-grade metamorphic gneisses.

3. Methods

In order to identify the provenance of sediments transported in the Rhône river, this study uses several fingerprinting techniques. As this research focuses on a large-scale provenance tracing, it is not useful to establish fingerprints for each individual lithology. This would be complicated given the large number and similarity of some of the exposed lithologies. Instead, a tributary sampling approach was chosen, which is based on the assumption that the sediment at the outlet of a tributary basin represents a natural mixture of all upstream lithologies (e.g., von Blanckenburg, 2005; Garzanti et al., 2012; Vale et al., 2016). Using such an approach, small-scale lithological differences are averaged out, and the focus can be set upon large-scale erosional and sedimentary dynamics. We assume no short-term (within year or between year) variability in sub-basin response that might cause the composition of a deposit to vary. Given the hydrological and litho-tectonic architecture of the basin (Stutenbecker et al., 2016), it is sufficient to group the tributary basins into sources within the Penninic domain, the Helvetic nappes and the External massifs including the sub-Penninic Gotthard nappe (Fig. 1). While the Helvetic nappes and External massifs are rather homogenous in terms of their lithologic architecture (mostly carbonates and metagranitoids, respectively), the Penninic domain is made up of a wider range of rocks, including oceanic sediments, oceanic basement, continental basement and its sedimentary cover. However, at this scale of investigation we consider the different

lithologies as one unit, because most Penninic tributary basins drain all of these lithologies, and the presence of ophiolites offers great discriminatory potential of this unit to the other two, ophiolite-free units.

To provide pure endmember fingerprints of the respective unit, tributary basins chosen for sediment fingerprinting should ideally drain only one of the three litho-tectonic units described above. Catchments with mixed provenance such as the Drance basin that is underlain by Penninic rocks and units of the External massifs were thus excluded from this analysis (Fig. 1). Within each litho-tectonic unit five to six basins were selected to test whether different tributary basins draining source rocks of the same domain have comparable fingerprints. These are, for the External massifs, the Baltschiederbach, Goneri, Lonza, Massa, Münstigerbach and Wysswasser rivers, for the Penninic nappes, the Borgne, Navisence, Printse, Turtmanna and Vispa rivers and for the Helvetic nappes the Avançon, Dala, Lixerne, Morge and Sionne rivers (see Fig. 1 for locations). Furthermore, six sampling locations were chosen along the Rhône trunk river to trace provenance changes downstream. In addition to the samples taken for sediment fingerprinting, eight supplementary locations from the Rhône river and nine additional tributary basins were sampled for terrestrial cosmogenic nuclide (TCN) analysis in order to constrain absolute denudation rates (Fig. 1). For consistency, the samples taken from within the Rhône river are numbered 1 to 14 from up- to downstream. The tributary river samples were collected at the river outlet as close as possible to the confluence with the Rhône river to make sure that they comprise all upstream lithologies, but far enough upstream to prevent

contamination with floodplain sediment of the main Rhône river. The samples were first sieved and weighed for grain size analysis using sieves of 31.5, 16, 8, 4, 2, 1, 0.5, 0.25, 0.125 and 0.063 mm openings (see supplementary data 1) and subsequently separated into three groups for the analysis: <0.063 mm for bulk geochemistry, 0.063 – 0.25 mm for heavy mineral analysis and petrography and 0.25 – 0.4 mm for TCN extraction.

3.1 Sediment fingerprinting

The sediment composition was characterized using three different fingerprinting techniques: Framework petrography, heavy mineral analysis and bulk geochemistry.

Framework petrography data were obtained from thin sections of the grain size fraction 0.063 – 0.25 mm. At least 250 grains per thin section were counted under a polarization microscope. Following the classification schemes introduced by Garzanti & Vezzoli (2003) and Garzanti et al. (2012) monocrystalline quartz (Q), polycrystalline quartz including chert (Q_p), feldspar (Fsp), carbonate rock fragments (L_c), sedimentary and low-rank metasedimentary rock fragments (L_{sm}), medium- and high-rank felsic metamorphic rock fragments (L_{mf}), and metabasite rock fragments (L_{mb}) were counted.

Heavy minerals were separated using lithium heteropolytungstate (LST fast float, ρ= 2.85 g/cm^3) from the grain size fraction of 0.063 – 0.25 mm. The extracted dense minerals were prepared as polished blocks and analysed using a QEMSCAN® facility installed at the Department of Earth Sciences at the University of Geneva, Switzerland. The system is featured by the field emission gun (FEG)

electron source while mineral phase identification relies on the combination of back-scattered electron (BSE) values and X-ray spectra, giving information on the elemental composition of the spectrum acquisition point (Gottlieb et al., 2000). Individual X-ray spectra were compared to a library of known spectra and a mineral name was assigned to each individual acquisition point. The X-ray EDS spectra library, initially provided by the manufacturer, has been developed further in-house using a variety of natural standards. Measurements were performed on carbon-coated polished sections. Analytical conditions included a high vacuum and an acceleration voltage of 25 kV with probe current of 10 nA. X-ray acquisition time was 10 ms per pixel using a point-spacing of 5 µm.

The QEMSCAN® results included compositional area-percentage data of up to 134 different grain types. This amount was substantially reduced to a final number of 14 categories by removing "spurious" grains (Garzanti & Andò, 2007) such as intergrown light minerals (quartz, feldspar, evaporites, carbonates), clay minerals (illite, kaolinite), phyllosilicates (chlorite, biotite, muscovite), anthropogenically introduced grains (corundum, steel), and by grouping together certain mineral groups (see supplementary data 2). These data were also used to calculate the heavy mineral concentration (HMC) as introduced by Garzanti & Andò (2007). The fraction <0.063 mm was chosen for whole rock geochemical analysis using lithium borate fusion coupled with ICP-ES at the Acmelabs in Canada. The analytical package included the major element oxides SiO_2, Al_2O_3, CaO, Fe_2O_3, MgO, Na_2O, K_2O, TiO_2, P_2O_5, MnO, Cr_2O_3, as well as the trace elements Ba, Ni, Sr, Zr, Y, Nb and Sc. All results were corrected for the loss of ignition (LOI).

The three fingerprinting methods applied in this study produce a large amount of data, for which it is difficult to identify compositional patterns by conventional visualization methods such as pie charts or histograms (Vermeesch & Garzanti, 2015). In order to identify key characteristics such as diagnostic fingerprinting proxies or inter-sample variability, a statistical treatment of the raw data is essential. Because compositional data are most commonly measured relative to each other (e.g. in percent or parts per million), they are inevitably correlated with each other and sum up to a constant sum of 1 or 100%. In this case, principal component analysis (PCA) is recommended to reduce data dimensionality, visualize data variance and to identify sample groupings and key variables (Gabriel, 1971; Aitchison, 1983, 1990; Aitchison & Greenacre, 2002). Compositional biplots were created using a centred log-ratio data transformation in the software CoDaPack (Comas & Thió-Henestrosa, 2011). Where compositional data were zero, the value was replaced with 0.001 (Martín-Fernández et al., 2003; Garzanti et al., 2010).

3.2 Statistical source discrimination

A three-step statistical analysis was used to identify fingerprinting proxies with a maximum discriminatory potential suitable as an input for a mixing model (Collins et al., 1996; Cooper et al., 2014; Laceby et al., 2015). The first requirement is the mass conservation from source to sink. In nature, however, this condition is not always fulfilled. For example, heavy minerals might get enriched in fluvial systems through hydrological sorting (Garzanti et al., 2009) or cleaved rock fragments might be physically destroyed during

transport (Garzanti et al., 2015). Mass conservation was verified by calculating the minimum and maximum values of both source and in-stream sediments. If the minimum or maximum value of a component in the in-stream sediment was out of the source range, the component was removed. Secondly, the non-parametric Kruskal-Wallis H-test identifies components that provide significant discrimination between samples from the three sources (Collins et al., 1996; Collins & Walling, 2002; Evrard et al., 2011). The H-test was chosen as it does not require data that follow a Gaussian distribution. Components that did not pass the Kruskal-Wallis H-test (i.e., p-values > 0.05) were excluded from the mixing model input parameters. Finally, amongst the mass-conservative and discriminatory components, stepwise linear discrimination analysis (LDA) was used to determine a minimum number of components, which in combination provide the greatest discrimination between the source groups. This is achieved by stepwise minimization of Wilk's lambda (Collins et al., 1996; Haddadchi et al., 2014; Laceby & Olley, 2015; Palazón et al., 2015). All statistical analyses were performed in R version 3.2.2.

3.3 Mixing modelling

Mixing models are commonly used in provenance studies to determine the relative contributions of source end members to a sediment population (Collins et al., 1996; Weltje, 1997; Garzanti et al., 2012). Here, the mixing model equation developed by Laceby & Olley (2015) is solved with the Optquest algorithm in Oracle's software CrystalBall. The Optquest algorithm identifies the

percentage contributions of endmember sources, which best reproduce the observed in-stream sediment composition by minimizing the difference between simulated and observed composition (MMD).

$$MMD = \sum_{i=1}^{n}(C_i - (\sum_{s=1}^{m} P_s \cdot S_{si})) \div C_i \quad \text{(eq.1)}$$

where n is the number of fingerprinting components chosen as input parameters, i is a fingerprinting component (e.g. CaO), C_i is the concentration of the component i in the in-stream sample, m is the number of sources in the catchment (in this case = 3), P_s the relative contribution (%) of each source s, and S_{si} the concentration of component i in the source s.

3.4 ^{10}Be-based denudation rates

Catchment-wide denudation rates were calculated from the concentration of the terrestrial cosmogenic nuclide (TCN) ^{10}Be in quartz. In quartz grains, ^{10}Be is mainly produced from ^{16}O through spallation reactions triggered by secondary cosmic rays (Lal & Peters, 1967). The concentration of ^{10}Be in quartz increases with the time of exposure to the cosmic ray shower on the Earth's surface. It is therefore inversely proportional to the denudation rate (Lal, 1991). The production rate of TCN from cosmic rays depends on the elevation and the latitude of the studied location (Lal, 1991), and needs to be calculated on a pixel-by-pixel basis for each river

catchment. Additionally, the production of TCN in mountainous settings can decrease significantly depending on the shielding of the location due to surrounding topography (topographic shielding) as well as snow and ice cover (Dunne et al., 1999; Gosse & Philipps 2001).

Sample preparation was accomplished using protocols reported in (Akçar et al., 2012). Accordingly, ca. 50 grams of pure quartz was extracted from the 0.25 – 0.4 mm grain size fractions using magnetic separation, followed by successive leaching with hydrochloric, phosphoric and hydrofluoric acid, as well as aqua regia. The purified quartz was then spiked with a ^{9}Be carrier and dissolved in concentrated hydrofluoric acid. Beryllium was stepwise extracted from this solution using anion and cation exchange column chemistry following the protocol of Akçar et al. (2012). Final precipitates were oxidized and pressed into targets for accelerator mass spectrometry (AMS) analysis . ^{10}Be/^{9}Be ratios were measured using the 500 kV TANDY AMS facility at ETH Zürich (Christl et al., 2013). The obtained ratios were normalized with the ETH in-house standard S2007N (Kubik & Christl, 2010) and corrected using a full process blank ^{10}Be/^{9}Be ratio of $2.28 \pm 0.14 \times 10^{-15}$.

Although around 10 kg of material per sample was collected from the carbonate-rich Helvetic catchments, less than 20 grams of material was left after the first leaching step with hydrochloric acid, which is insufficient for ^{10}Be measurement. For future studies, it might be advisable to use cosmogenic ^{36}Cl instead to obtain denudation rates.

The local production rate and topographic shielding were calculated based on a 20-m-resolution digital elevation model of Switzerland in the CAIRN calculator (Mudd et al., 2016). Within this routine, the

default parameters given in Mudd et al. (2016) were used and reported in Table 4. Snow cover was accounted for using an elevation-dependent mean annual snow-cover database for Switzerland (Auer, 2003). This dataset was subsequently converted into snow water equivalent thickness (SWE, g/cm^2) using an empirical relationship (Jonas et al., 2009). Spatially averaged snow-shielding factors were then estimated for each catchment, considering the estimated mean annual SWE and a neutron attenuation length of 160 g/cm^2 (Lal, 1991) and incorporated into the CAIRN routine. The production rate was set to zero for permanently glaciated areas, which were extracted from the Geological Map of Switzerland (Swiss Federal Office of Topography Swisstopo, 2011). Note that the correction factors related to snow and ice shielding are assumed to be conservative due to possible spatial and temporal variations in snow thickness and persistence as well as glacier extent over the timescale integrated by the TCN signal (i.e. $10^2 – 10^3$ y)

The denudation rates were multiplied with catchment size and an estimated mean density of 2650 kg/m^3 in order to obtain absolute sediment loads in kg/yr for each catchment (see, e.g. Hinderer et al., 2013; Cruz Nunes et al., 2015; Wittmann et al., 2016).

Note that by sampling sediment at the basin outlet, the concentration of ^{10}Be yields a spatially averaged denudation rate of all erosional processes in the catchment upstream of the sampling location (Brown et al., 1995; Bierman & Steig, 1996; Granger et al., 1996). Geomorphic decoupling of some of the sediment sources and contributions of large volumes of glaciogenic material might add a bias in the application of the methodology. We thus emphasize that

the values reported in this paper represent upper bounds for erosional fluxes.

4. Results and interpretation

4.1 Sediment fingerprinting

The External massifs shed quartzofeldspathic sands with both medium- to high-rank felsic metamorphic (mostly meta-granites) and low-rank metasedimentary rock fragments. The relative abundance of heavy minerals is moderate (mean HMC 4.6) and the suites are dominated by epidote and amphibole. The Penninic nappes supply lithoquartzofeldspathic metamorphiclastic sands with minor metacarbonate and metabasite rock fragments. Heavy minerals are abundant (very rich with a mean HMC 15.4) and related suites are also dominated by epidote and amphibole. Detritus from the Helvetic nappes is carbonaticlastic with minor low-rank metasedimentary, mostly pelitic rock fragments and very low quartz and feldspar contents. The heavy mineral concentrations are low (mean HMC 1.4) and the suites are dominated by iron oxides and pyrite with minor apatite, amphibole and epidote. A summary of all fingerprinting data can be found in the supplementary data 2.

Biplots facilitate the pinpointing of the compositional differences between samples derived from the External massifs, the Penninic and the Helvetic nappes (Fig. 2). Key components characterizing the Penninic sediment are for example metabasite rock fragments, tourmaline, olivine, pyroxene, Cr_2O_3 and Ni, which can be expected

in sediments partially derived from ophiolitic sources. The dominance of carbonates in the Helvetic sediments is expressed by key components such as carbonate rock fragments, wollastonite, CaO and Sr. Sediment derived from the External massifs is characterized by components such as quartz, feldspar, high-rank felsic metamorphic rock fragments, titanite, zircon and monazite. The PCA results confirm that different tributary basins of the same litho-tectonic unit have comparable compositional signatures and that there is a significant variability between the three main litho-tectonic units (Fig. 2).

4.2 Source discrimination

The principle of mass conservation was fulfilled for all components except for the sulphide traps in the heavy mineral dataset (see supplementary data 2). Kyanite, apatite, olivine, zircon, rutile, tourmaline and Ni did not pass the Kruskal-Wallis H-test (Table 1). Stepwise LDA suggests that the combination of the components CaO, Fe_2O_3, L_{sm}, L_c and Na_2O provides the best discrimination between the three endmember sources and so these should be used in the mixing model (Table 2). However, in order to compare the different methods and to test the influence of statistical pre-selection of components with a theoretically high discriminator potential onto the results, the mixing model was run separately with all components as well as with the pre-selected components for all three datasets.

4.3 Mixing models

The results obtained from mixing modelling differ quite substantially depending on which of the three fingerprinting methods was used (Table 3). However, within each fingerprinting technique, the choice of input parameters (all or statistically selected ones), does not change the results significantly (Table 3). When the petrographic dataset is used as an input, results suggest that material derived from the External massifs is the dominant constituent of the Rhône river sediments (61 – 69%), followed by Helvetic material (18 – 20%) and Penninic material (13 – 19%). When using the bulk geochemical data obtained from the <0.063 mm grain size fraction as an input, the modelled results shift towards a higher Helvetic (38 – 43%) and very low Penninic (2.6 – 4%) contribution. This could be an expression of the easier mechanical destruction of carbonate material, which accordingly could be found more frequently in finer grain sizes. However, the most striking difference occurs when the heavy mineral dataset is used, in which case the result suggests that 100% of the sediment close to the Rhône river delta has Penninic sources. The most likely interpretation of this deviating value initiates from the fact that Penninic samples tend to have much higher heavy mineral concentrations (HMC) than samples from the External massifs or the Helvetic nappes (see supplementary data 2). Here, a correction factor could be applied (Garzanti et al., 2008), where both hydraulic sorting processes and the actual difference of heavy mineral fertility of the different source rocks are considered. Even if this could be accomplished with sufficient detail, the very low HMC of Helvetic material and its consequent dilution or absence in Rhône river heavy mineral suites would remain evident. In addition, heavy minerals show the lowest discriminatory potential amongst the three

fingerprinting datasets. For example, in the compositional biplots, only ~60% of data variance is explained by the first two principal components, whereas this percentage is much higher for the geochemical (82%) and the petrographic (85%) datasets (Fig. 2). Most heavy minerals failed the Kruskal-Wallis H-test (Table 1), indicating that their concentrations in the source sediments are not significantly different enough to provide a suitable fingerprint. In stepwise LDA, samples were always correctly classified based on their geochemical and petrographic compositions, but not based on their heavy mineral concentration (Table 2).

It can therefore be concluded that fingerprinting in the Rhône basin works best with proxies derived from framework petrography or bulk geochemistry. This is reflected in the stepwise LDA (Table 2), which amongst the entire dataset (petrography, geochemistry and heavy minerals) produced the best results with a combination of petrographical and geochemical proxies only ($CaO + Fe_2O_3 + L_{sm} + L_c + Na_2O$). Using these proxies as inputs, the model output suggests that at the river site closest to the Rhône delta in Lake Geneva, the Rhône's fine sediment (<0.250 mm) is composed of 57% detritus derived from the External massifs, 23% of Penninic material and 20% of Helvetic material. Given the differences in methods and definition of the source areas, our results are in line with those of Garzanti et al. (2012), who suggested that Rhône sands were dominated by External massif material (~75%).

Although the goodness-of-fit achieved using pre-selected components from the entire dataset ($CaO + Fe_2O_3 + L_{sm} + L_c + Na_2O$) seems to be satisfactory, great care should be taken when interpreting such measures of model performance, as they have been found to be

not truly indicative or even misleading in some cases (Garzanti et al., 2012; Laceby & Olley, 2015). As suggested by Garzanti et al. (2012), attention should be given to the geological significance of a model rather than relying on numerical measures only. Accordingly, we decided to validate our model by calculating source contributions for samples located at different positions within the Rhône river (Fig. 3). Because of the overall architecture of the basin, this allows us to test whether the model predicts the logically expected incorporation of litho-tectonic units into the watershed at certain sampling locations. Using the parameters CaO + Fe_2O_3 + L_{sm} + L_c + Na_2O, the model predicts 100% External massif contribution for the Rhône-1 sample, where the Rhône river only drains External massif units (Fig. 3). At location Rhône-6, a minor contribution of Helvetic material is predicted, which is geologically plausible, as some carbonate cover of the European basement is preserved in the External massifs as well. At location Rhône-11, where finally all of the three litho-tectonic units outcrop within the watershed, the model correctly predicts contributions of all three sources. Accordingly, it can be concluded that the model performance is also satisfactory in geological terms.

4.4 ^{10}Be-based denudation rates

^{10}Be concentrations of the tributary basin samples yield denudation rates between 0.19 ± 0.04 mm/yr (Mundbach) and 7.43 ± 2.04 mm/yr (Illgraben) (Table 4). Spatially averaged denudation rates along the Rhône river vary substantially between 0.13 ± 0.03 and 1.40 ± 0.32 mm/yr with an average value of ca. 0.87 mm/yr. The large variability

of ^{10}Be concentrations even in samples collected in close proximity indicates that Rhône sediments are not well mixed (Fig. 4).

Absolute sediment loads derived from the calculated denudation rates range from 0.012 ± 0.003 x 10^9 kg/yr (Mundbach) to 3.101 ± 0.613 x 10^9 kg/yr (Drance). At the outlet of the basin, a total sediment flux of 15.977 ± 3.216 x 10^9 kg/yr was obtained (Table 5).

The extreme high denudation rate calculated for the Illgraben sample is a statistical outlier. Sediment in the Illgraben catchment is mainly derived from frequent rock falls on the north-western flank and debris flows on south-eastern flank (Schlunegger et al., 2009; Bennett et al., 2012; 2013). These massive erosional events supply large volumes of material within a very short time span (Berger et al., 2011), which explains the exceptionally high denudation rates. Denudation rates of sediment taken from the main Rhône river, however, never exceed 1.40 mm/yr, indicating that the input of Illgraben material with extreme low-^{10}Be concentrations does not noticeably influence the ^{10}Be-budget on the investigated spatial and temporal scale (Fig. 4). All other calculated denudation rates are comparable to catchment-wide denudation rates that were previously reported from neighbouring regions in the Alps (Wittmann et al., 2007; Norton et al., 2010). In order to compare the denudation rates between the litho-tectonic units defined in the compositional analysis, the tributaries were grouped together according to their dominant bedrock geology (Fig. 5). Results show that mean denudation rates in the Penninic tributaries (1.23 ± 0.71 mm/yr) are slightly, but not significantly higher than in the External massifs (0.81 ± 0.39 mm/yr).

5. Discussion

Discrepancy of denudation rates and mixing modelling results

Results from compositional mixing modelling suggest that 57% of the mixed sediment reaching Lake Geneva is composed of material derived from the External massifs, whereas the Helvetic nappes and the Penninic nappes contribute 20% and 23%, respectively. Generally, sediment supply volumes should scale with catchment size (Wilson, 1973; Milliman & Syvitski, 1992; Syvitski et al., 2003; Church, 2017) at least to the point at which a basin area begins to contain significant contributions from two or more lithologies with relatively different erodibilities (Church, 2017). Considering that ca. 56% of the Rhône basin is underlain by Penninic lithologies and only 27% by rocks of the External massifs, Penninic material seems to be relatively underrepresented in the sediment budget. In a previous study, Garzanti et al. (2012) came to similar conclusions. These authors suggested that higher denudation rates in the Northeast of the Rhône basin may lead to an overrepresentation of material derived from the External massifs. This explanation would be supported by the observation that the highest modern rock uplift rates are measured in the area of the External massifs (Schlatter et al., 2005) and a strong correlation of rock uplift and denudation rate has been reported in the Central Alps (Wittmann et al., 2007). Our results, however, do not show significantly higher denudation rates in tributaries located in the External massifs (Fig. 5). On the contrary, some of the highest denudation rates have been obtained for tributary basins located in the Penninic nappes.

This suggests either that a different process is responsible for the observed sediment composition or that the spatial pattern of modern denudation is substantially different from the longer-term one obtained through TCN analysis. The ^{10}Be-based denudation rates integrate over a time span of ca. 100 – 3000 years (assuming a cosmic ray absorption depth of ca. 600 mm). In order to explain significant changes of denudation rates in modern times a process acting on much shorter time scales than this integration time would be required, and this process could possibly be directly observable today. In the following part, we will explore potential solutions to explain the observed discrepancy.

Textural differences of the sediments

It is well established that rocks and the sediments they produce may have substantially different erodibilities and subsequent stabilities during transport. In the study area, the erodibilities of the rocks were classified to be "very low" for the granites of the External massifs, "low" for the metamorphic rocks of Penninic nappes and "medium" for the Helvetic carbonates by Kühni & Pfiffner (2001), based on the geotechnical map of Switzerland by Niggli & de Quervain (1936). It thus seems possible that the less stable Helvetic and Penninic rocks break down faster compared to the sediments derived from the External massifs, both during weathering and during transport. As a consequence, sediment produced from the Penninic or Helvetic nappes could already be finer grained when entering the Rhône river, and subsequently get enriched in the very fine suspended or even dissolved sediment load during transport.

Grain size analysis prior to mineral separation does not support this hypothesis. The grain size distributions of the samples taken at the tributary river outlets are largely comparable (Fig. 6). There is, in contrast, some evidence supporting that certain lithologies are being enriched in the finer fraction during transport in the Rhône river. The analysis of the <0.063 mm fraction yielded higher contributions of Helvetic carbonates (>40%) than in the 0.063 – 0.25 mm fraction (<20%). However, Penninic material is not enriched, but in contrast virtually absent in the <0.063 mm (<5%) compared to the 0.063 – 0.25 mm fraction (>10%). Therefore, a dominant control of textural characteristics onto the sediment composition appears unlikely to explain the observed pattern.

Misfit of modern and longer-term denudation and sediment loads

Several studies already reported on discrepancies between modern (measured) and longer-term (TCN-derived) sediment loads related to the misfit of timescales (e.g. Schaller et al., 2001; Covault et al., 2013; Wittmann et al., 2016). In Europe, sediment discharges derived from TCN analysis were shown to exceed modern measurements by 1.5 – 4 times in the Loire, Meuse, Neckar and Regen rivers (Schaller et al., 2001) and by 2 – 3 times in the Po river basin (Wittmann et al. 2016). These authors relate the mismatch to the fact that gauging data, in contrast to TCN-derived loads, do not account (a) for potentially significant bed load (Turowski et al., 2010), (b) for material derived from infrequent, but large erosional events such as landslides (Schaller et al., 2001), or (c) for sediment storage between source and sink (Covault et al., 2013). In particular, sediment loads

derived from ^{10}Be concentrations only account for sediment production in the catchment, and are not necessarily sensitive to sediment storage. Sediment leaving a basin may have the same ^{10}Be concentration irrespective of the presence or amount of sediment storage in the upstream area of the sampling point (Wittmann et al., 2016).

In the upper Rhône basin, one gauging station near Porte du Scex, ca. 5 km upstream of the river mouth, records suspended sediment concentrations. Accordingly, sediment discharge can only be compared on a basin scale, not on the tributary basin scale. Measured mean annual suspended sediment discharge at Porte du Scex is around 2 x 10^9 kg/yr, although for 2012 and 2013, higher values of up to 6 x 10^9 kg/yr were recorded (Swiss Federal Office of the Environment, 2017). In contrast, the total sediment load at the basin outlet calculated from ^{10}Be concentrations (Table 5) amounts to ca.16 x 10^9 kg/yr, i.e. 3 – 8 times more than the measured value.

Since the portion of sediment discharge through bed load transport in the upper Rhône river is estimated to amount to only 9 – 11% of the total sediment load (Schlunegger & Hinderer, 2003; Hinderer et al., 2013), this cannot fully explain the mismatch between the two datasets. Likewise, sediment input from landslides generally has a negligible effect in larger catchments such as the upper Rhône basin, although it may disturb the TCN signal in smaller basins that are dominated by mass wasting processes such as the Illgraben (Niemi et al., 2005; Yanites et al., 2009). Sediment storage, however, is known to have been significant in the upper Rhône basin throughout the Quaternary. For example, a valley fill of more than 800 m thickness was identified in the main Rhône valley using gravimetric and

seismic methods (Kissling & Schwendener, 1990; Pfiffner et al., 1997). Smaller-scale storage exists in the deposits of glacial tills, rock glaciers or along hillslopes in some of the tributary catchments (Otto et al., 2009). In general, it is well established that only a percentage of the sediment eroded from a basin reaches the catchment outlet, and this percentage tends to decrease, to potentially small fractions, with increasing basin size (Walling, 1983). The reason for this effect is debated (e.g. Parsons et al., 2006) but is generally thought to relate to an increase of accommodation space as basin area increases (de Vente & Poesen, 2005; Fryirs et al., 2007, Blöthe & Korup, 2013; Fryirs, 2013). Accordingly, the wide and flat valley bottom of the main Rhône river could provide significant storage capacities for sediment, which could explain some of the mismatch between the observed and calculated sediment loads. However, storage along the main river could not explain the observed pattern of sediment composition, as it is unlikely that the main floodplain would preferentially store detritus from the Penninic nappes, and not from the External massifs or the Helvetic nappes. Furthermore, the storage ability and capacity of the Rhône river floodplain is probably significantly reduced today due to the correction and channelization of the river course.

The largest tributary basins (e.g. the Vispa, Drance and Borgne basins) are all located in the Penninic nappes and, in theory, could accommodate, and thus store, larger volumes of sediment than the comparatively smaller tributaries located in the Helvetic nappes or the External massifs. For instance, Fig. 7 shows that the length of the trunk river is positively correlated to catchment size. Sediments have to travel longer distances in the large Penninic basins with a higher

probability of being trapped along the way compared to the shorter rivers of the Helvetic and especially the External massifs tributaries. In the Penninic Borgne basin, for instance, sediment accumulation rates as high as 9 cm/yr were measured along some braided river sections between 1959 and 2014 (Bakker et al., 2017). However, the deposition along the river beds or on the hillslopes may not be permanent and sediment may be remobilized. In the absence of comprehensive modern measurements of sediment storage in different basins, this effect and its impact onto the basin-wide sediment budget remains hard to quantify.

In addition to natural, potentially only temporary sediment storage along the hillslopes or river beds, sediment storage and removal by human activities could play a significant role in the study area. The upper Rhône basin accommodates some of Europe's largest hydroelectric power plants and their connected water storage reservoirs (Anselmetti et al., 2007; Fatichi et al., 2015). Most of the structures, and in particular the facilities with the largest storage capacities, were constructed in the large southern tributaries draining the Penninic nappes in the middle of the 20th century (Loizeau & Dominik, 2000). Dams lead to the direct trapping of very fine-grained sediments in the connected water reservoirs (Vörösmarty et al., 1997; 2003; Kummu & Varis, 2007; Syvitski & Milliman, 2007) and, in the absence of reservoir flushing flows, to the permanent storage of sediment. In the upper Rhône basin, only six reservoirs have storage capacities large enough to be managed without regular flushing. These are the Mauvoisin, Les Toules, Lac de Dix, Moiry, Mattmark and Emosson reservoirs, of which the first five are located in the Penninic nappes and the latter one in the External massifs.

Total sediment accumulation rates from these reservoirs amount to a (semi)-permanent storage of ca. 0.4 x 10^9 kg/yr (Beyer-Portner, 1998; Hinderer et al., 2013), of which 0.38 x 10^9 kg/yr (94%) are accounted for by the five Penninic reservoirs (Table 6).

In addition to water management, the upper Rhône basin is subject to intense sediment mining. According to the extraction volumes published by Kündig et al. (1997), between 0.5 and 1.7 x 10^9 kg/yr of modern fluvial sediments are permanently removed from the study area (Table 7), of which the majority is extracted along the main Rhône river (0.3 – 0.8 x 10^9 kg/yr). Additional volumes of 0.1 to 0.6 x 10^9 kg/yr are extracted in the Penninic tributaries, 0.02 to 0.08 x 10^9 kg/yr in the Helvetic tributaries and 0.05 to 0.2 x 10^9 kg/yr in the tributaries located in the External massifs (Table 7). Sediment to be used as construction material is one of the most important resources in Switzerland. Due to the steadily increasing demand and price, it is likely that the amount of extraction sites as well as the extracted volumes increased in recent years, which is why we consider the maximum volumes reported by Kündig et al. (1997) to be closer to reality than the minimum estimates.

In summary, our estimates suggest that up to 2 x 10^9 kg/yr of sediment is removed from the upper Rhône basin by human activities, which is the same amount as it is being discharged at Porte du Scex (Fig. 8). The relative underrepresentation of Penninic material as observed in the sediment composition could be a consequence of focused human impact in the Penninic tributaries, where up to ca. 1 x 10^9 kg/yr are either stored in the reservoirs or extracted at mining sites.

Overestimation of denudation rates and sediment loads

Even though we inferred that artificial sediment storage and extraction significantly impact sediment fluxes in the study area with respect to the total sediment discharge, the volumes compiled here fail to fully explain the mismatch between the calculated and the measured sediment loads (Fig. 8).

Therefore, an additional explanation lies in the uncertainty of the calculated denudation rates. The basic principle of catchment-wide denudation is the assumption that the entire catchment supplies sediment to the sampled sediment at the outlet according to the local denudation rates. However, given the strong human impact due to semi-permanent storage, water management and sediment extraction, this principle might be violated. Additional complications in interpreting the TCN-derived sediment loads could arise from the relatively large proportion of glaciated surface in the upper Rhône basin (ca. 14%). Glaciogenic material derived from sub- or proglacial areas usually has very low ^{10}Be concentrations (e.g. Delunel et al., 2014). If glaciers contribute large amounts of this sediment to the system, the resulting catchment-wide denudation rates are apparently high, but do not necessarily represent a real spatial average of the basin (Godard et al., 2012). In the Central Alps, glacial retreat increased substantially in response to short-term climatic changes within the last decades (e.g., Fischer et al., 2014). As glaciers retreat, they expose large proglacial areas covered by unconsolidated, easily erodible sediment. Accordingly, sediment discharge from glacial areas was found to have increased recently in several locations in the upper Rhône basin (Micheletti et al., 2015; Lane et al, 2016; Delaney

et al., 2017). However, in order to quantify the actual contributions of glacial sources and to understand the limits they might impose, individual sub-basins should be explored in greater detail.

6. Conclusions

In this study a multi-method approach was used to fingerprint the three main lithological units present in the upper Rhône river basin. Results show that granitoids of the External massifs, carbonates of the Helvetic nappes and mixed meta-oceanic and continental basement rocks of the Penninic nappes have distinct petrographical, chemical, and, to some extent, mineralogical fingerprints. Compositional modelling showed that sediment close to the basin outlet is composed of 57% External massif material, followed by 23% Penninic material and 20% Helvetic material. The concentrations of the TCN ^{10}Be in fluvial sand suggest a different contribution, in which absolute denudation rates and thus sediment loads are actually highest in the southern Penninic tributaries. Overall, the sediment discharge calculated from denudation rates at the basin outlet is around 16 x 10^9 kg/yr in contrast to a measured value of only 2 x 10^9 kg/yr.

We hypothesized that the overestimation of TCN-derived sediment loads could be a combination of two processes. On the one hand, we showed that significant amounts of sediment are stored within or extracted from the system by water management and sediment extraction, in particular in the Penninic unit. Overall, an amount of up to 2 x 10^9 kg/yr seems to be diverted from the natural flux by human activities. On the other hand, the TCN-derived denudation

rates and resulting sediment loads could be overestimated due to the strong human impact and due to high inputs of glaciogenic sediment from retreating glaciers. Here, the role of glacial sources within individual tributary basins should be further investigated.

Contributions

L. Stutenbecker performed field work, sample preparations, laboratory work for TCN analysis, petrographical and statistical analyses under the supervision of F. Schlunegger. R. Delunel assisted with the calculations and interpretation of denudations rates from measured ^{10}Be concentrations. B. Šegvić supervised T. Silva and L. Stutenbecker during the QEMSCAN® analysis at University of Geneva. T. Silva, S. Girardclos, M. Bakker, A. Costa, S.N. Lane, J.-L. Loizeau and P. Molnar gave valuable input during different stages of this work, including field work and discussion. N. Akçar and M. Christl were involved in the preparation and measurement of TCN samples in the TCN laboratory at University of Bern and the AMS facility at ETH Zürich, respectively.

Acknowledgements

This study has been funded by the Sinergia grant number 147689 awarded to F. Schlunegger, S. Girardclos, S. Lane, J.-L- Loizeau and P. Molnar by the Swiss National Science Foundation. L. Stutenbecker thanks J. Patrick Laceby and Pieter Vermeesch for fruitful discussions and valuable suggestions about statistical data treatment and mixing modelling. We would like to thank the entire TCN team at the University Bern for support in the laboratory. Constructive reviews and helpful comments by Giovanni Vezzoli,

two anonymous reviewers and the editors are gratefully acknowledged.

References

Aitchison, J., 1990. Relative variation diagrams for describing patterns of compositional variability. Mathematical Geology 22, 487–511.

Aitchison, J., 1983. Principal Component Analysis of Compositional Data. Biometrika 70, 57–65.

Aitchison, J., Greenacre, M., 2002. Biplots of compositional data. Applied Statistics 51, 375–392.

Akçar, N., Deline, P., Ivy-Ochs, S., Alfimov, V., Hajdas, I., Kubik, P.W., Christl, M., Schlüchter, C., 2012. The AD 1717 rock avalanche deposits in the upper Ferret Valley (Italy): A dating approach with cosmogenic 10Be. Journal of Quaternary Science 27, 383–392.

Anselmetti, F.S., Bühler, R., Finger, D., Girardclos, S., Lancini, A., Rellstab, C., Sturm, M., 2007. Effects of Alpine hydropower dams on particle transport and lacustrine sedimentation. Aquatic Sciences 69, 179–198.

Auer, M., 2003. Regionalisierung von Schneeparametern—Eine Methode zur Darstellung von Schneeparametern im Relief. MSc thesis University of Bern, 97 pages.

Baartman, J.E.M., Masselink, R., Keesstra, S.D., Temme, A.J.A.M., 2013. Linking landscape morphological complexity and sediment

connectivity. Earth Surface Processes and Landforms 38, 1457–1471.

Bennett, G.L., Molnar, P., Eisenbeiss, H., Mcardell, B.W., 2012. Erosional power in the Swiss Alps: Characterization of slope failure in the Illgraben. Earth Surface Processes and Landforms 37, 1627–1640.

Bennett, G.L., Molnar, P., McArdell, B.W., Schlunegger, F., Burlando, P., 2013. Patterns and controls of sediment production, transfer and yield in the Illgraben. Geomorphology 188, 68–82.

Berger, C., McArdell, B.W., Schlunegger, F., 2011. Sediment transfer patterns at the Illgraben catchment, Switzerland: Implications for the time scales of debris flow activities. Geomorphology 125, 421–432.

Bernet, M., Brandon, M.T., Garver, J.I., Molitor, B., 2004. Downstream Changes of Alpine Zircon Fission-Track Ages in the Rhône and Rhine Rivers. Journal of Sedimentary Research 74, 82–94.

Beyer-Portner, N., 1998. Erosion des bassins versant alpins suisses par ruissellement de surface. PhD thesis, Ecole Polytechnique Federal, Lausanne, Switzerland.

Bierman, P.R., Steig, E.J., 1996. Estimating rates of denudation using cosmogenic isotope abundances in sediment. Earth Surface Processes and Landforms 21, 125-139.

Bini, A., Buoncristiani, J.F., Couterrand, S., D., E., Felber, M., Florineth, D., Graf, H.R., Keller, O., Kelly, M., Schlüchter, C., Schoeneich, P., 2009. Switzerland during the last glacial maximum.

Swisstopo, 1:50000, Wabern.

Blöthe, J.H., Korup, O., 2013. Millennial lag times in the Himalayan sediment routing system. Earth and Planetary Science Letters 382, 38–46.

Brown, E.L., Stallard, R.F., Larsen, M.C., Raisbeck, G.M., Yiou, F., 1995. Denudation rates determined from the accumulation of in situ-produced 10Be in the Luquillo Experimental Forest, Puerto Rico. Earth and Planetary Science Letters 129, 193-202.

Champagnac, J.D., Molnar, P., Sue, C., Herman, F., 2012. Tectonics, climate, and mountain topography. Journal of Geophysical Research Solid Earth 117, B02403.

Christl, M., Vockenhuber, C., Kubik, P.W., Wacker, L., Lachner, J., Alfimov, V., Synal, H.A., 2013. The ETH Zurich AMS facilities: Performance parameters and reference materials. Nuclear Instruments and Methods in Physics Research Section B: Beam Interaction with Materials and Atoms 294, 29–38.

Church, M., 2017. Interpreting sediment yield scaling. Accepted in Earth Surface Processes and Landforms, doi: 10.1002/esp.4165.

Collins, A.L., Walling, D.E., 2002. Selecting fingerprint properties for discriminating potential suspended sediment sources in river basins. Journal of Hydrology 261, 218–244.

Collins, A.L., Walling, D.E., Leeks, G.J.L., 1996. Composite fingerprinting of the spatial source of fluvial suspended sediment : a case study of the Exe and Severn river basins, United Kingdom. Géomorphologie : relief, processus, environnement 2, 41–53.

Comas, M., Thió-Henestrosa, S., 2011. CoDaPack 2.0: a stand-alone multi-platform compositional software, in: Egozcue, J.J., Tolosana-Delgado, R., Ortego, M.I. (Eds.), CoDaWork'11: 4th International Workshop on Compositional Data Analysis. Saint Feliu de Guixols, Girona, Spain.

Cooper, R.J., Krueger, T., Hiscock, K.M., Rawlins, B.G., 2014. Sensitivity of fluvial sediment source apportionment to mixing model assumptions : A Bayesian model comparison. Water Resources Research 50, 9031–9047.

Costa, A., Molnar, P., Stutenbecker, L., Bakker, M., Silva, T.A., Schlunegger, F., Lane, S.N., Loizeau, J.-L., Girardclos, S., 2017. Temperature signal in suspended sediment export from an Alpine catchment. Hydrology and Earth System Sciences Discussions. 1–30. doi:10.5194/hess-2017-2

Covault, J.A., Craddock, W.H., Romans, B.W., Fildani, E., Gosai, M, 2003. Spatial and Temporal Variations in Landscape Evolution: Historic and Longer-Term Sediment Flux through Global Catchments. The Journal of Geology 121, 35-56.

Cruz Nunes, F., Delunel, R., Schlunegger, F., Akcar, N., Kubik, P.W., 2015. Bedrock bedding, landsliding and erosional budgets in the Central European Alps. Terra Nova 27, 370-378.

Dearing, J.A., Jones, R.T., 2003. Coupling temporal and spatial dimensions of global sediment flux through lake and marine sediment records. Global and Planetary Change 39, 147–168.

Delaney, I., Bauder, A., Huss, M., Weidmann, Y., 2017. Proglacial

erosion rates and processes in a glacierized catchment in the Swiss Alps. Accepted in Earth Surface Processes and Landforms, doi: 10.1002/esp.4239

Delunel, R., van der Beek, P.A., Bourlès, D.L., Carcaillet, J., Schlunegger, F., 2014. Transient sediment supply in a high-altitude Alpine environment evidenced through a 10Be budget of the Etages catchment (French Western Alps). Earth Surface Processes and Landforms 39, 890-899.

de Vente, J., Poesen, J., 2005. Predicting soil erosion and sediment yield at the basin scale: Scale issues and semi-quantitative models. Earth-Science Reviews 71, 95–125.

Diekmann, B., Hofmann, J., Henrich, R., Fütterer, D.K., Röhl, U., Wei, K.Y., 2008. Detrital sediment supply in the southern Okinawa Trough and its relation to sea-level and Kuroshio dynamics during the late Quaternary. Marine Geology 255, 83–95.

Dunne, J., Elmore, D., Muzikar, P., 1999. Scaling factors for the rates of production of cosmogenic nuclides for geometric shielding and attenuation at depth on sloped surfaces. Geomorphology 27, 3-11.

Evrard, O., Navratil, O., Ayrault, S., Ahmadi, M., Némery, J., Legout, C., Lefèvre, I., Poirel, A., Bonté, P., Esteves, M., 2011. Combining suspended sediment monitoring and fingerprinting to determine the spatial origin of fine sediment in a mountainous river catchment. Earth Surface Processes and Landforms 36, 1072–1089.

Fatichi, S., Rimkus, S., Burlando, P., Bordoy, R., Molnar, P., 2015. High-resolution distributed analysis of climate and anthropogenic

changes on the hydrology of an Alpine catchment. Journal of Hydrology 525, 362–382.

Florineth, D., Schlüchter, C., 1998. Reconstructing the Last Glacial Maximum (LGM) ice surface geometry and flowlines in the Central Swiss Alps. Eclogae Geologicae Helvetiae 91, 391–407.

Fryirs, K., 2013. (Dis)Connectivity in catchment sediment cascades: A fresh look at the sediment delivery problem. Earth Surface Processes and Landforms 38, 30–46.

Fryirs, K., Brierley, G.J., Preston, N.J., Kasai, M., 2007. Buffers, barriers and blankets: The (dis)connectivity of catchment-scale sediment cascades. Catena 70, 49–67.

Gabriel, K.R., 1971. The Biplot Graphic Display of Matrices with Application to Principal Component Analysis. Biometrika 58, 453–467.

Garzanti, E., Andò, S., 2007. Heavy mineral concentration in modern sands: implications for provenance interpretation. Developments in Sedimentology 58, 517–545.

Garzanti, E., Andò, S., Vezzoli, G., 2009. Grain-size dependence of sediment composition and environmental bias in provenance studies. Earth Planetary and Science Letters 277, 422–432.

Garzanti, E., Andò, S., Vezzoli, G., 2008. Settling equivalence of detrital minerals and grain-size dependence of sediment composition. Earth Planetary and Science Letters 273, 138–151.

Garzanti, E., Resentini, A., Andò, S., Vezzoli, G., Pereira, A.,

Vermeesch, P., 2015. Physical controls on sand composition and relative durability of detrital minerals during ultra-long distance littoral and aeolian transport (Namibia and southern Angola). Sedimentology 62, 971–996.

Garzanti, E., Resentini, A., Vezzoli, G., Andò, S., Malusà, M.G., Padoan, M., 2012. Forward compositional modelling of Alpine orogenic sediments. Sedimentary Geology 280, 149–164.

Garzanti, E., Resentini, A., Vezzoli, G., Andò, S., Malusà, M.G., Padoan, M., Paparella, P., 2010. Detrital Fingerprints of Fossil Continental-Subduction Zones (Axial Belt Provenance, European Alps). Journal of Geology 118, 341–362.

Garzanti, E., Vezzoli, G., 2003. A Classification of Metamorphic Grains in Sands Based on their Composition and Grade. Journal of Sedimentary Research 73, 830–837.

Godard, V., Burbank, D.W., Bourlès, D.L., Bookhagen, B., Braucher, R., Fisher, G.B., 2012. Impact of glacial erosion on 10Be concentrations in fluvial sediments of the Marsyandi catchment, central Nepal. Journal of Geophysical Research 117, F03013, doi:10.1029/2011JF002230.

Goodbred, S.L., Kuehl, S.A., 1999. Holocene and modern sediment budgets for the Ganges-Brahmaputra river system: Evidence for highstand dispersal to flood-plain, shelf, and deep-sea depocenters. Geology 27, 559–562.

Gosse, J.C., Phillips, F.M., 2001. Terrestrial in situ cosmogenic nuclides: theory and application. Quaternary Science Reviews 20,

1475-1560.

Gottlieb, P., Wilkie, G., Sutherland, D., Ho-Tun, E., Suthers, S., Perera, K., Jenkins, B., Spencer, S., Butcher, A., Rayner, J., 2000. Using quantitative electron microscopy for process mineralogy applications. The Journal of The Minerals, Metals & Material Society 52, 24–25.

Granger, D.E., Kirchner, J.W., Finkel, R., 1996. Spatially averaged long-term erosion rates measured from in situ-produced cosmogenic nuclides in alluvial sediment. The Journal of Geology 104, 249-257.

Haddadchi, A., Olley, J., Laceby, P., 2014. Accuracy of mixing models in predicting sediment source contributions. Science of the Total Environment 497–498, 139–152.

Harrison, C.G.A., 2000. What factors control mechanical erosion rates? International Journal of Earth Sciences 88, 752–763.

Hay, W.W., Wold, C.N., Herzog, J.M., 1992. Preliminary mass-balanced 3-D reconstructions of the Alps and surrounding areas during the Miocene, in: Pflug, R., Harbaugh, J.W. (Eds.), Computer Graphics in Geology. Lecture Notes in Earth Sciences. Springer, Berlin, Heidelberg, pp. 99–110.

Herwegh, M., Berger, A., Baumberger, R., Wehrens, P., Kissling, E., 2017. Large-Scale Crustal-Block-Extrusion During Late Alpine Collision. Scientific Reports 7, 413.

Hinderer, M., 2012. From gullies to mountain belts: A review of sediment budgets at various scales. Sedimentary Geology 280, 21–59.

Hinderer, M., Kastowski, M., Kamelger, A., Bartolini, C., Schlunegger, F., 2013. River loads and modern denudation of the Alps - A review. Earth-Science Reviews 118, 11–44.

Joerin, U.E., Stocker, T.F., Schlüchter, C., 2006. Multicentury glacier fluctuations in the Swiss Alps during the Holocene. The Holocene 16, 697–704.

Jonas, T., Marty, C., Magnusson, J., 2009. Estimating the snow water equivalent from snow depth measurements in the Swiss Alps. Journal of Hydrology 378, 161–167.

Kelly, M.A., Buoncristiani, J.F., Schlüchter, C., 2004. A reconstruction of the last glacial maximum (LGM) ice-surface geometry in the western Swiss Alps and contiguous Alpine regions in Italy and France. Eclogae Geologicae Helvetiae 97, 57–75.

Kissling, E., Schwendener, H., 1990. The Quaternary sedimentary fill of some Alpine valleys by gravity modelling. Eclogae Geologicae Helvetiae 83, 311-321.

Korup, O., 2009. Linking landslides, hillslope erosion, and landscape evolution. Earth Surface Processes and Landforms 34, 1315–1317.

Kubik, P.W., Christl, M., 2010. 10Be and 26Al measurements at the Zurich 6 MV Tandem AMS facility. Nuclear Instruments and Methods in Physics Research Section B: Beam Interaction with Materials and Atoms 268, 880–883.

Kühni, A., Pfiffner, O.A., 2001. The relief of the Swiss Alps and adjacent areas and its relation to lithology and structure: topographic analysis from a 250-m DEM. Geomorphology 41, 285-307.Kündig,

R., Mumenthaler, T., Eckardt, P., Keusen. H.R., Schindler, C., Hofmann, F., Vogler, R., Guntli, P., 1997. Die mineralischen Rohstoffe der Schweiz. Schweizerische Geotechnische Kommission, Zürich, 522 p.

Kummu, M., Varis, O., 2007. Sediment-related impacts due to upstream reservoir trapping, the Lower Mekong River. Geomorphology 85, 275–293.

Laceby, J.P., McMahon, J., Evrard, O., Olley, J., 2015. A comparison of geological and statistical approaches to element selection for sediment fingerprinting. Journal of Soils and Sediments 15, 2117–2131.

Laceby, J.P., Olley, J., 2015. An examination of geochemical modelling approaches to tracing sediment sources incorporating distribution mixing and elemental correlations. Hydrological Processes 29, 1669-1685.

Lal, D., 1991. Cosmic ray labeling of erosion surfaces: in situ nuclide production rates and erosion models. Earth and Planetary Science Letters 104, 424–439.

Lal, D., Peters, B., 1967. Cosmic rays produced radioactivity on the Earth, in: Handbuch Der Physik, Vol. XLVI/2, Springer, Berlin. pp. 551–612.

Lane, S.N., Bakker, M., Balin, D., Lovis, B., Regamey, B., 2014. Climate and human forcing of Alpine river flow, in: Schleiss, A.J., De Cesare, G., Franca, M.J., Pfister, M. (Eds.), River Flow 2014, 7–15.

Lane, S.N., Bakker, M., Gabbud, C., Micheletti, N., Saugy, J.-N., 2017. Sediment export, transient landscape response and catchment-scale connectivity following rapid climate warming and Alpine glacier recession. Geomorphology 277, 210–227.

Loizeau, J.L., Dominik, J., 2000. Evolution of the upper Rhone river discharge and suspended sediment load during the last 80 years. Aquatic Sciences 62, 54–67.

Ludwig, W., Probst, J.L., 1996. Predicting the oceanic input of organic carbon by continental erosion. Global Biogeochemical Cycles 10, 23–41.

Martín-Fernández, J., Barceló-Vidal, C., Pawlowsky-Glahn, V., 2003. Dealing with Zeros and Missing Values in Compositional Data Sets Using Nonparametric Imputation. Mathematical Geology 35, 253–278.

McLaughlin, C.J., Smith, C.A., Buddemeier, R.W., Bartley, J.D., Maxwell, B.A., 2003. Rivers, runoff, and reefs. Global and Planetary Change 39, 191–199.

Meile, T., Boillat, J.L., Schleiss, A.J., 2011. Hydropeaking indicators for characterization of the Upper-Rhone River in Switzerland. Aquatic Sciences 73, 171–182.

Meybeck, M., 2003. Global analysis of river systems: from Earth system controls to Anthropocene syndromes. Philosophical transactions of the Royal Soceity of London. Series B, Biological sciences 358, 1935–55.

Micheletti, N., Lambiel, C., Lane, S., 2015. Investigating decadal-

scale geomorphic dynamics in an alpine mountain setting. Journal of Geophysical Research: Earth Surface 120, 2155–2175.

Micheletti, N., Lane, S.N., 2016. Water yield and sediment export in small, partially glaciated Alpine watersheds in a warming climate. Water Resources Research 52, 4924–4943.

Milliman, J.D., Syvitski, J.P.M., 1992. Geomorphic/Tectonic Control of Sediment Discharge to the Ocean: The Importance of Small Mountainous Rivers. Journal of Geology 100, 525–544.

Molnar, P., Anderson, R.S., Anderson, S.P., 2007. Tectonics, fracturing of rock, and erosion. Journal of Geophysical Research: Earth Surface 112, 1–12.

Montgomery, D.R., Brandon, M.T., 2002. Topographic controls on erosion rates in tectonically active mountain ranges. Earth and Planetary Science Letters 201, 481–489.

Mudd, S.M., Harel, M.A., Hurst, M.D., Grieve, S.W.D., Marrero, S.M., 2016. The CAIRN method: Automated, reproducible calculation of catchment-averaged denudation rates from cosmogenic nuclide concentrations. Earth Surface Dynamics 4, 655–674.

Niggli, P., de Quervain, F.D., 1936. Geotechnische Karte der Schweiz. Schweizerische Geotechnische Kommission, Kümmerly and Frey, Geotechnischer Verlag, Bern. (In German)

Norton, K.P., von Blanckenburg, F., DiBiase, R., Schlunegger, F., Kubik, P.W., 2011. Cosmogenic 10Be-derived denudation rates of the Eastern and Southern European Alps. International Journal of Earth Sciences 100, 1163–1179.

Norton, K.P., von Blanckenburg, F., Kubik, P.W., 2010. Cosmogenic nuclide-derived rates of diffusive and episodic erosion in the glacially sculpted upper Rhone Valley, Swiss Alps. Earth Surface Processes and Landforms 35, 651–662.

Otto, J.C., Schrott, L., Jaboyedoff, M., Dikau, R., 2009. Quantifying sediment storage in a high alpine valley (Turtmanntal, Switzerland). Earth Surface Processes and Landforms 34, 1726-1742.

Palazón, L., Gaspar, L., Latorre, B., Blake, W.H., Navas, A., 2015. Identifying sediment sources by applying a fingerprinting mixing model in a Pyrenean drainage catchment. Journal of Soils and Sediments 15, 2067–2085.

Parsons, A.J., Wainwright, J., Brazier, R.E., Powell, D.M., 2006. Is sediment delivery a fallacy? Earth Surface Processes and Landforms 31, 1325–1328.

Phillips, J.D., 2005. Weathering instability and landscape evolution. Geomorphology 67, 255–272.

Pfiffner, O.A., Heitzmann, P., Lehner, P., Frei, W., Pugin, A., Felber, M., 1997. Incision and backfilling of Alpine valleys: Pliocene, Pleistocene and Holocene processes, in: Pfiffner, O.A., Lehner, P., Heitzmann, P., Müller, S., Steck, A. (Eds.), Deep structure of the Swiss Alps: Results of NRP 20, Birkhäuser Verlag, Basel, 265–288.

Schaller, M. von Blanckenburg, F., Hovius, N., Kubik, P.W., 2001. Large-scale erosion rates from in situ-produced cosmogenic nuclides in European river sediments. Earth and Planetary Science Letters 188, 441-458.

Schildgen, T.F., Phillips, W.M., Purves, R.S., 2005. Simulation of snow shielding corrections for cosmogenic nuclide surface exposure studies. Geomorphology 64, 67–85.

Schlatter, A., Schneider, D., Geiger, A., Kahle, H.G., 2005. Recent vertical movements from precise levelling in the vicinity of the city of Basel, Switzerland. International Journal of Earth Sciences 94, 507–514.

Schlunegger, F., Badoux, A., McArdell, B.W., Gwerder, C., Schnydrig, D., Rieke-Zapp, D., Molnar, P., 2009. Limits of sediment transfer in an alpine debris-flow catchment, Illgraben, Switzerland. Quaternary Science Reviews 28, 1097–1105.

Schlunegger, F., Hinderer, M., 2003. Pleistocene/Holocene climate change, re-establishment of fluvial drainage network and increase in relief in the Swiss Alps. Terra Nova 15, 88-95.

Schmid, S.M., Fügenschuh, B., Kissling, E., Schuster, R., 2004. Tectonic map and overall architecture of the Alpine orogen. Eclogae Geologicae Helvetiae 97, 93–117.

Schmid, S.M., Pfiffner, O.A., Froitzheim, N., Schönborn, G., Kissling, E., 1996. Geophysical -geological transect and tectonic evolution of the Swiss-Italian Alps. Tectonics 15, 1036–1064.

Snelgrove, P.V.R., 1997. The Importance of Marine Sediment Biodiversity in Ecosystem Processes. Ambio 26, 578–583.

Stallard, R.F., 1998. Terrestrial sedimentation and the carbon cycle: Coupling weathering and erosion to carbon burial. Global Biogeochemical Cycles 12, 231–257.

Stutenbecker, L., Costa, A., Schlunegger, F., 2016. Lithological control on the landscape form of the upper Rhône Basin, Central Swiss Alps. Earth Surface Dynamics 4, 253–272.

Summerfield, M.A., Hulton, N.J., 1994. Natural controls of fluvial denudation rates in major world drainage basins. Journal of Geophysical Research 99, 13871–13883.

Swiss Committee on Dams, 2011. Dams in Switzerland: Source for Worldwide Swiss Dam Engineering. http://www.swissdams.ch/index.php/en/swiss-dams/map-of-dams-in-switzerland

Swiss Federal Office of the Environment, 2017. Hydrologisches Jahrbuch der Schweiz 2016. Annual report of the Bundesamt für Umwelt BAFU, Bern, Switzerland, 34 p. (In German or French)

Swiss Federal Office of Topography Swisstopo, 2011. Geologische/tektonische/hydrogeologische Karte der Schweiz 1:500000. Swisstopo,Wabern.Syvitski, J.P.M., Milliman, J.D., 2007. Geology, Geography, and Humans Battle for Dominance over the Delivery of Fluvial Sediment to the Coastal Ocean. Journal of Geology 115, 1–19.

Syvitski, J.P.M., Peckham, S.D., Hilberman, R., Mulder, T., 2003. Predicting the terrestrial flux of sediment to the global ocean: A planetary perspective. Sedimentary Geology 162, 5–24.

Tebbens, L.A., Kroonenberg, S.B., van den Berg, M.W., 1995. Compositional variation of detrital garnets in Quaternary Rhine , Meuse and Baltic River sediments in the Netherlands. Geologie en

Mijnbouw/Netherlands Journal of Geocsciences 74, 213–224.

Trümpy, R., 1960. Paleotectonic evolution of the Central and Western Alps. Bulletin of the Geological Society of America 71, 843–908.

Tucker, G.E., Bras, R.L., 1998. Hillslope processes, drainage density, and landscape morphology. Water Resources Research 34, 2751–2764.

Turowski, J., Rickenmann, D., Dadson, S.J., 2010. The partitioning of the total sediment load of a river into suspended load and bedload: a review of empirical data. Sedimentology 57, 1126-1146.

Vale, S.S., Fuller, I.C., Procter, J.N., Basher, L.R., Smith, I.E., 2016. Application of a confluence-based sediment-fingerprinting approach to a dynamic sedimentary catchment, New Zealand. Hydrological Processes 30, 812–829.

Vermeesch, P., Garzanti, E., 2015. Making geological sense of "Big Data" in sedimentary provenance analysis. Chemical Geology 409, 20–27.

von Blanckenburg, F., 2005. The control mechanisms of erosion and weathering at basin scale from cosmogenic nuclides in river sediment. Earth and Planetary Science Letters 237, 462–479.

Vörösmarty, C.J., Meybeck, M., Fekete, B., Sharma, K., Green, P., Syvitski, J.P.M., 2003. Anthropogenic sediment retention: Major global impact from registered river impoundments. Global and Planetary Change 39, 169–190.

Vörösmarty, C.J., Sharma, K.P., Fekete, B.M., Copeland, A.H., Holden, J., Marble, J., Lough, J.A., 1997. The Storage and Aging of Continental Runoff in Large Reservoir Systems of the World. Ambio 26, 210–219.

Walling, D.E., 1983. The Sediment Delivery Problem. Journal of Hydrology 65, 209–237.

Weber, C., Peter, A., Zanini, F., 2007. Spatio-temporal analysis of fish and their habitat: A case study on a highly degraded Swiss river system prior to extensive rehabilitation. Aquatic Sciences 69, 162–172.

Weltje, G.J., 1997. End-member modeling of compositional data: Numerical-statistical algorithms for solving the explicit mixing problem. Mathematical Geology 29, 503–549.

Willett, S.D., 1999. Orogeny and orography: The effects of erosion on the structure of mountain belts. Journal of Geophysical Research 104, 28957–28981.

Wilson, L., 1973. Variations in mean annual sediment yield as a function of mean annual precipitation. American Journal of Science, 273, 335-349.

Wittmann, H., von Blanckenburg, F., Kruesmann, T., Norton, K.P., Kubik, P.W., 2007. Relation between rock uplift and denudation from cosmogenic nuclides in river sediment in the Central Alps of Switzerland. Journal of Geophysical Research: Earth Surface 112, F04010, doi:10.1029/2006JF000729

Wittmann, H., Malusà, M.G., Resentini, A., Garzanti, E.,

Niedermann, S., 2016. The cosmogenic record of mountain erosion transmitted across a foreland basin: Source-to-sink analysis of in-situ ^{10}Be, ^{26}Al and ^{21}Ne in sediment of the Po river catchment. Earth and Planetary Science Letters 452, 258-271.

Fig. 1: Location and tectonic map of the upper Rhône basin showing the general litho-tectonic architecture of the basin (Federal Office of Topography Swisstopo, 2011), the main Rhône river, its tributary rivers and watershed outlines, sampling locations, glaciers (Federal Office of Topography Swisstopo, 2011), hydropower dams with significant storage capacity and their catchments (Swiss Committee on Dams, 2011; Hinderer et al., 2013) and sites of sediment extraction (Kündig et al., 1997). The abbreviations refer to the names of the rivers: Ava = Avançon, Aeg = Aegene, Bal = Baltschiederbach, Bie = Bietschbach, Bli = Blinne, Bor = Borgne, Dal = Dala, Dra = Drance, Far = Farne, Gam = Gamsa, Gon = Goneri, Ill = Illgraben, Lix = Lixerne, Lon = Lonza, Mas = Massa, Mor = Morge, Mun = Mundbach, Mün = Münstigerbach, Nav = Navisence, Pri = Printse, Sio = Sionne, Tri = Trient, Tur = Turtmanna, Vis = Vispa, Wys = Wysswasser.

Fig. 2: Compositional biplots derived from principle component analysis for the petrographic dataset (a), the heavy mineral dataset (b) and the geochemical dataset (c). The coloured dots represent the tributary river samples. The length of the red rays is proportional to the amount of variation explained by the corresponding element. The abbreviations of the fingerprinting elements in a) and b) refer to the following petrographical or mineralogical proxies: Q = monocrystalline quartz, Q_p = polycrystalline quartz, Fsp = feldspar, L_c = carbonate rock fragments, L_{sm} = sedimentary and low-rank metasedimentary rock fragments, L_{mf} = medium- and high-rank felsic metamorphic rock fragments, L_{mb} = metabasite rock fragments, Grt = garnet, Amph = amphibole, Ky = kyanite, Ap = apatite, Mon = monazite, FeOx = iron oxides, Ep = epidote, Ol = olivine, Px = pyroxene, Rut = rutile, Tit = titanite, Tour = tourmaline, Wol = wollastonite, Zr = zircon.

Fig. 3: Schematic representation of the Rhône river (not to scale) showing the tributary rivers sampled for compositional analysis (arrow length is proportional to basin size). Pie charts represent the modelled relative contributions of the three sources to sediment sampled at different locations within the Rhône river.

Fig. 4: Schematic representation of the Rhône river and its tributary basins (not to scale) showing the development of denudation rates (in mm/yr) downstream the Rhône river. The length of the arrows refers to the size of the tributary basins.

Fig. 5: Boxplots displaying the range of denudation rates between tributaries draining the External massifs and the Penninic nappes. The extremely high denudation rate obtained for the Illgraben sample was excluded (see text).

Fig. 6: Ternary plot showing the grain size distributions of the collected tributary samples. For the full dataset, see supplementary data 1.

Fig. 7: Plot showing the strong correlation of catchment size and the length of the trunk river for all tributary basins investigated in this study.

Fig. 8: Schematic source-to-sink model for the upper Rhône basin including the measured sediment discharge at the basin outlet, the total sediment production calculated from cosmogenic nuclides and the numbers on human-induced sediment diversion compiled in this study.

Table 1: Results of the Kruskal-Wallis H-test for each element. Elements with a p-value > 0.05 (asterisked) are considered to be not statistically different between the three source units.

Fingerprinting method	Elements	H value	p value
Framework Petrography	Monocrystalline quartz (Q)	12.876	0.002
	Polycrystalline quartz (Q_p)	12.053	0.002
	Feldspar (Fsp)	13.365	0.001
	Carbonate rock fragments (L_c)	13.504	0.001
	Sedimentary and low-rank metasedimentary rock fragments (L_{sm})	9.965	0.007
	Medium- and high-rank felsic metamorphic rock fragments (L_{mf})	10.067	0.007
	Metabasite rock fragments (L_{mb})	14.379	0.001
Heavy mineral analysis	Garnet (Grt)	8.355	0.015
	Amphibole (Amph)	9.380	0.009

	Kyanite (Ky)	1.086	0.581*
	Apatite (Ap)	2.780	0.249*
	Monazite (Mon)	9.388	0.009
	Iron oxides (FeOx)	9.360	0.009
	Epidote (Ep)	9.380	0.009
	Olivine (Ol)	2.647	0.266*
	Pyroxene (Px)	6.512	0.039
	Rutile (Rut)	2.340	0.310*
	Titanite (Tit)	10.519	0.005
	Tourmaline (Tour)	4.705	0.095*
	Wollastonite (Wol)	13.325	0.001
	Zircon (Zr)	3.782	0.151*
Bulk geochemistry	SiO_2	13.346	0.001
	Al_2O_3	7.088	0.029
	Fe_2O_3	9.722	0.008
	MgO	7.512	0.023
	CaO	13.346	0.001
	Na_2O	13.346	0.001
	K_2O	9.440	0.009

TiO_2	9.051	0.011
P_2O_5	9.912	0.007
MnO	11.522	0.003
Cr_2O_3	10.341	0.006
Ba	9.118	0.010
Ni	4.318	0.115*
Sr	10.110	0.006
Zr	6.569	0.037
Y	10.110	0.006
Nb	8.051	0.018
Sc	8.581	0.014

Table 2: Elements selected through stepwise linear discriminant analysis (LDA). The error refers to the percentage of samples not correctly classified by the respective step.

Fingerprinting method	Output elements	Error	Wilk's lambda
Framework petrography	1) L_c	6.3%	0.06398
	2) $L_c + L_{sm}$	0%	0.00536
	3) $L_c + L_{sm} + Q_p$	0%	0.00230
	4) $L_c + L_{sm} + Q_p + L_{mb}$	0%	**0.00112**
Heavy mineral analysis	1) Tit	20%	0.26412
	2) Tit + Amph	6.7%	0.09884
	3) Tit + Amph + Mon	6.7%	0.03748
	4) Tit + Amph + Mon + Ep	6.7%	**0.01177**
Bulk geochemistry	1) CaO	6.3%	0.03346
	2) $CaO + Fe_2O_3$	0%	0.00653
	3) $CaO + Fe_2O_3 + Na_2O$	0%	0.00265
	4) $CaO + Fe_2O_3 + Na_2O + Al_2O_3$	0%	0.00149

	5) $CaO + Fe_2O_3 + Na_2O + Al_2O_3 + Cr_2O_3$	0%	**0.00074**
All data	1) CaO	6.7%	0.03495
	2) $CaO + Fe_2O_3$	0%	0.00688
	3) $CaO + Fe_2O_3 + L_{sm}$	0%	0.00242
	4) $CaO + Fe_2O_3 + L_{sm} + L_c$	0%	0.00112
	5) $CaO + Fe_2O_3 + L_{sm} + L_c + Na_2O$	0%	**0.00034**

Table 3: Contribution of the three source units to the sediment at the Rhône outlet as modelled based on different fingerprinting elements as input parameters. The goodness of fit (GOF) is a measure for model performance used by Laceby & Olley (2015).

Fingerprinting method	Input parameters	External massifs (%)	Penninic nappes (%)	Helvetic nappes (%)	GOF
Framework petrography	$L_c + L_{sm} + Q_p + L_{mb}$	61.8 ± 2.1	22.1 ± 2	16.2 ± 1.2	53%
	all elements	68 ± 2.5	11.7 ± 3.6	20.3 ± 1.1	55%
Heavy mineral analysis	Tit + Amph + Mon +Ep	100	0	0	54%
	all elements	100	0	0	52%
Bulk geochemistry	$CaO + Fe_2O_3 + Na_2O + Al_2O_3 + Cr_2O_3$	54.8 ± 1	2.6 ± 1	42.6 ± 1	78%
	all elements	48.2 ± 1	4 ± 1.1	47.8 ± 2.8	74%

All data	**$CaO + Fe_2O_3 + L_{sm}$**	**56.9 ± 9.6**	**23.4 ± 2.3**	**19.7 ± 1.0**	**74%**	**$+ L_c + Na_2O$**

Table 4: Summary of factors relevant for the ^{10}Be analysis and interpretation. The 1-sigma ^{10}Be uncertainty includes AMS, production and muon uncertainties. All calculation were based on the default parameters given in the CAIRN routine (Mudd et al., 2016), including 1.39 Myr for the half-life of ^{10}Be, 2.65 g/cm^3 for the density of quartz and 4.30 at/g/yr as sea level high latitude production rate.

River sample	Material dissolved (g)	^{9}Be carrier added (mg)	^{10}Be concentration (x10^3 at/g)	Production scaling	Topographic shielding	Snow shielding	Ice extent correction	Denudation rate (mm/yr)
Aeg(ene)	44.93	0.1579	23.60 ± 2.55	6.34	0.926	0.869	0.924	0.55 ± 0.12
Bal(tschiederbach)	44.75	0.1562	26.04 ± 1.76	7.17	0.885	0.889	0.895	0.53 ± 0.10
Bie(tschbach)	44.80	0.1612	39.92 ± 1.40	6.63	0.876	0.908	0.944	0.34 ± 0.06
Bli(nne)	44.44	0.1980	22.24 ± 4.32	6.75	0.889	0.888	1.000	0.65 ± 0.18
Bor(gne)	44.81	0.1591	5.02 ± 0.47	7.11	0.931	0.907	0.849	2.74 ± 0.56
Dra(nce)	45.07	0.1596	7.44 ± 0.53	6.48	0.916	0.915	0.878	1.73 ± 0.34
Far(ne)	45.13	0.1600	12.51 ± 0.65	4.72	0.947	0.910	1.000	0.90 ± 0.18
Gam(sa)	45.36	0.1586	12.43 ± 0.70	6.14	0.934	0.893	0.996	1.13 ± 0.22
Gon(eri)	45.33	0.1591	16.21 ± 1.00	6.69	0.911	0.879	0.928	0.83 ± 0.16
Ill(graben)	45.09	0.1584	1.42 ± 0.27	4.63	0.884	0.921	1.000	7.43 ±2.04
Lon(za)	44.60	0.1592	12.13 ± 0.70	6.93	0.915	0.892	0.909	1.15 ± 0.22
Mas(sa)	44.58	0.1581	8.43 ± 1.11	9.70	0.925	0.866	0.551	1.36 ± 0.31
Mun(dbach)	44.71	0.1962	73.18 ± 8.08	6.62	0.853	0.893	1.000	0.19 ± 0.04
Mün(stigerbach)	45.55	0.1595	12.47 ± 0.79	7.27	0.917	0.878	0.892	1.14 ± 0.22

Nav(isence)	45.03	0.1604	11.04 ± 0.63	7.06	0.932	0.899	0.838	1.21 ± 0.23
Pri(ntse)	44.80	0.1587	25.45 ± 1.06	5.96	0.950	0.889	0.972	0.52 ± 0.10
Tri(ent)	45.13	0.1568	10.95 ± 1.41	5.01	0.900	0.918	0.898	0.94 ± 0.22
Tur(tmanna)	45.31	0.1597	24.63 ± 1.03	7.58	0.941	0.882	0.913	0.63 ± 0.12
Vis(pa)	45.39	0.1592	15.65 ± 0.87	8.65	0.915	0.899	0.817	1.00 ± 0.19
Wys(swasser)	45.89	0.1592	9.72 ± 0.77	8.63	0.926	0.865	0.642	1.23 ± 0.24
Rhône-1	45.59	0.1574	13.79 ± 1.30	7.20	0.914	0.851	0.875	0.96 ± 0.20
Rhône-2	45.08	0.1579	16.75 ± 1.68	6.40	0.921	0.857	0.933	0.77 ± 0.16
Rhône-3	44.88	0.1578	10.29 ± 1.30	6.73	0.924	0.856	0.872	1.23 ± 0.28
Rhône-4	45.08	0.1939	18.77 ± 2.42	6.47	0.920	0.858	0.901	0.67 ± 0.15
Rhône-5	45.34	0.1580	12.47 ± 1.33	6.26	0.920	0.86	0.896	0.97 ± 0.21
Rhône-6	44.82	0.1942	42.20 ± 4.66	7.05	0.922	0.854	0.791	0.28 ± 0.06
Rhône-7	44.87	0.1535	10-14 ± 0.75	6.83	0.919	0.856	0.845	1.22 ± 0.24
Rhône-8	45.27	0.1579	12.12 ± 0.83	7.38	0.914	0.852	0.831	1.07 ± 0.21
Rhône-9	45.02	0.1942	21.58 ± 2.48	7.14	0.917	0.854	0.860	0.60 ± 0.13
Rhône-10	44.62	0.1933	29.01 ± 8.57	7.01	0.918	0.856	0.873	0.45 ± 0.17
Rhône-11	44.98	0.1571	9.27 ± 1.20	6.96	0.919	0.856	0.873	1.40 ± 0.32
Rhône-12	49.97	0.1750	97.29 ± 10.17	6.75	0.923	0.858	0.887	0.13 ± 0.03
Rhône-13	45.16	0.1596	9.67 ± 1.03	6.36	0.920	0.863	0.902	1.28 ± 0.27
Rhône-14	45.34	0.1614	9.93 ± 0.77	6.23	0.920	0.862	0.907	1.23 ± 0.25

Table 5: Sediment yields calculated from the denudation rate obtained from TCN analysis and the catchment size. To calculate yields in kg/yr from volumes (m^3/yr), an average density of 2650 kg/m^3 was assumed.

River	Catchment size (km^2)	Denudation rate (mm/yr)	Sediment yield (x10^3 m^3/yr)	Sediment yield (x10^9 kg/yr)
Aeg(ene)	36.0	0.55 ± 0.12	20 ± 4	0.052 ± 0.011
Bal(tschiederbach)	42.6	0.53 ± 0.10	22 ± 4	0.060 ± 0.012
Bie(tschbach)	21.9	0.34 ± 0.06	7 ± 1	0.020 ± 0.004
Bli(nne)	18.3	0.65 ± 0.18	12 ± 3	0.032 ± 0.009
Bor(gne)	385.1	2.74 ± 0.56	1055 ± 217	2.795 ± 0.575
Dra(nce)	674.8	1.73 ± 0.34	1170 ± 231	3.101 ± 0.613
Far(ne)	29.0	0.90 ± 0.18	26 ± 5	0.069 ± 0.014
Gam(sa)	38.5	1.13 ± 0.22	43 ± 8	0.115 ± 0.022
Gon(eri)	40.0	0.83 ± 0.16	33 ± 7	0.088 ± 0.017
Ill(graben)	11.0	7.43 ±2.04	82 ± 22	0.217 ± 0.060
Lon(za)	161.5	1.15 ± 0.22	186 ± 36	0.492 ± 0.095
Mas(sa)	202.9	1.36 ± 0.31	275 ± 62	0.730 ± 0.165
Mun(dbach)	23.8	0.19 ± 0.04	4 ± 1	0.012 ± 0.003
Mün(stigerbach)	15.7	1.14 ± 0.22	18 ± 3	0.048 ± 0.009
Nav(isence)	255.8	1.21 ± 0.23	310 ± 59	0.821 ± 0.158

Pri(ntse)	72.1	0.52 ± 0.10	38 ± 7	0.100 ± 0.019
Tri(ent)	83.2	0.94 ± 0.22	78 ± 18	0.208 ± 0.048
Tur(tmanna)	108.0	0.63 ± 0.12	68 ± 13	0.181 ± 0.034
Vis(pa)	773.9	1.00 ± 0.19	772 ± 147	2.045 ± 0.389
Wys(swasser)	84.6	1.23 ± 0.24	104 ± 21	0.275 ± 0.055
Rhône-14	**4919.1**	**1.23 ± 0.25**	**6029 ± 1214**	**15.977 ± 3.216**

Table 6: Volumes and masses of sediment stored in large hydropower reservoirs without significant flushing. Volumes from Beyer-Portner (1998), published in Hinderer et al. (2013). The masses were calculated assuming a density of 1500 kg/m3.

Site	Unit	Sediment volume (m^3/yr)	Sediment mass (x10^9 kg/yr)
Lac d'Emosson	External massifs	15000	0.023
Lac des Dix	Penninic nappes	50000	0.075
Lac les Toules	Penninic nappes	1750	0.003
Lac de Mauvoisin	Penninic nappes	167800	0.252
Lac de Moiry	Penninic nappes	6000	0.009
Mattmarksee	Penninic nappes	26680	0.040
Total	**All**	**267230**	**0.401**

Table 7: Ranges of sediment extraction volumes at locations within the main Rhône river and its tributaries (based on a compilation of Kündig et al., 1997). Masses were calculated from the given volumes assuming a density of 1600 kg/m^3.

Site	Unit	Sediment volume (m^3/yr)	Sediment mass ($x10^9$ kg/yr)
Brig/Glis	Rhône river	10000 – 50000	0.016 – 0.080
Evionnaz	Rhône river	50000 – 1000000	0.080 – 0.160
Leuk	Rhône river	10000 – 50000	0.016 – 0.080
Martigny	Rhône river	10000 – 50000	0.016 – 0.080
Pfynwald	Rhône river	50000 – 1000000	0.080 – 0.160
Pfynwald	Rhône river	50000 – 1000000	0.080 – 0.160
Vionnaz	Rhône river	10000 – 50000	0.016 – 0.080
Baltschieder	External massifs	10000 – 50000	0.016 – 0.080
Fiesch	External massifs	10000 – 50000	0.016 – 0.080
Naters	External massifs	10000 – 50000	0.016 – 0.080
Chamoson	Helvetic nappes	10000 – 50000	0.016 – 0.080
Eison	Penninic nappes	10000 – 50000	0.016 – 0.080
Evolène	Penninic nappes	10000 – 50000	0.016 – 0.080
Gamsen	Penninic nappes	10000 – 50000	0.016 – 0.080
Hérémence	Penninic nappes	10000 – 50000	0.016 – 0.080
Stalden	Penninic nappes	10000 – 50000	0.016 – 0.080

Vollèges	Penninic nappes	10000 – 50000	0.016 – 0.080
Vollèges	Penninic nappes	10000 – 50000	0.016 – 0.080
Sum	Rhône river	190000 – 500000	0.304 – 0.800
Sum	External massifs	30000 – 150000	0.048 – 0.240
Sum	Helvetic nappes	10000 – 50000	0.016 – 0.080
Sum	Penninic nappes	70000 – 350000	0.112 – 0.560
Sum	**All**	**300000 – 1050000**	**0.480 – 1.680**

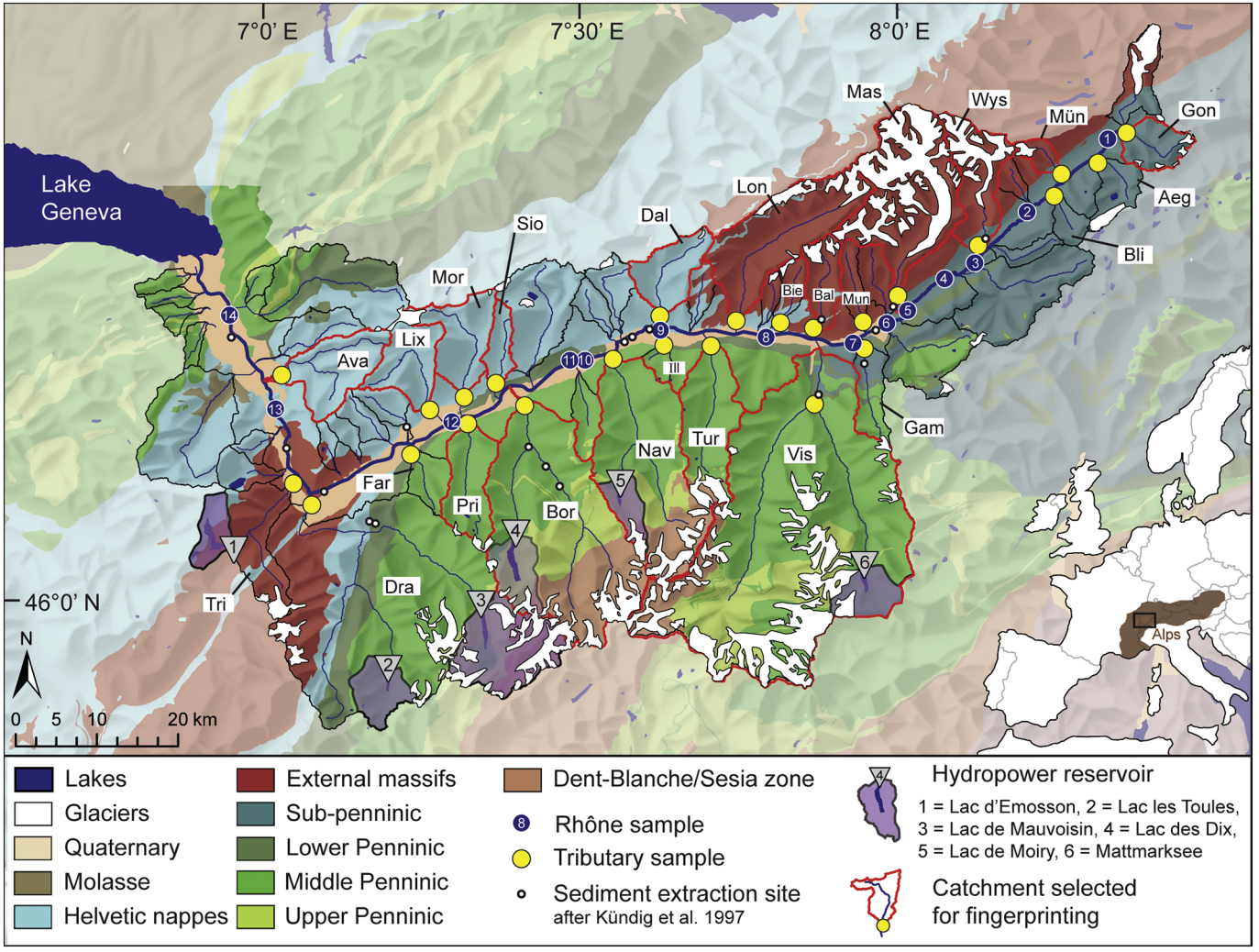
7°0' E
7°30' E
8°0' E
46°0' N
N
0 5 10 20 km
Lake Geneva
Mas
Wys
Mün
Gon
Aeg
Bli
Lon
Dal
Sio
Mor
Bie
Bal
Mun
Lix
Ava
Ill
Gam
Nav
Tur
Vis
Far
Pri
Bor
Dra
Tri
Alps
Lakes
Glaciers
Quaternary
Molasse
Helvetic nappes
External massifs
Sub-penninic
Lower Penninic
Middle Penninic
Upper Penninic
Dent-Blanche/Sesia zone
Rhône sample
Tributary sample
Sediment extraction site
after Kündig et al. 1997
Hydropower reservoir
1 = Lac d'Emosson, 2 = Lac les Toules,
3 = Lac de Mauvoisin, 4 = Lac des Dix,
5 = Lac de Moiry, 6 = Mattmarksee
Catchment selected
for fingerprinting

Figure 1

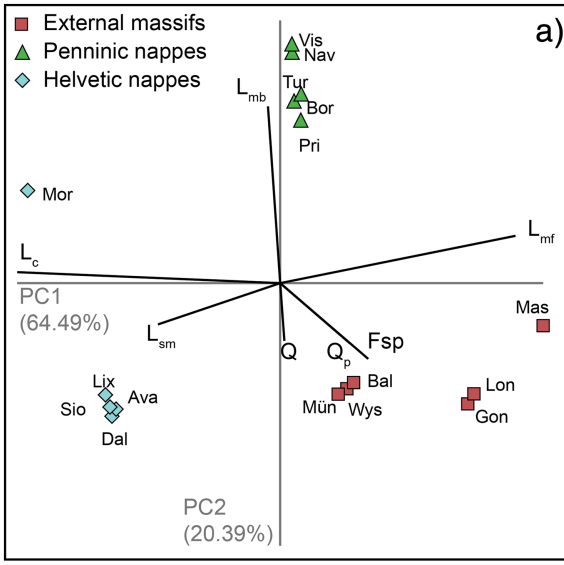
a)
External massifs
Penninic nappes
Helvetic nappes
Vis
Nav
Tur
Bor
Pri
L_{mb}
Mor
L_{mf}
L_c
PC1
(64.49%)
Mas
L_{sm}
Q
Q_p
Fsp
Bal
Lon
Lix
Ava
Sio
Mün
Wys
Gon
Dal
PC2
(20.39%)

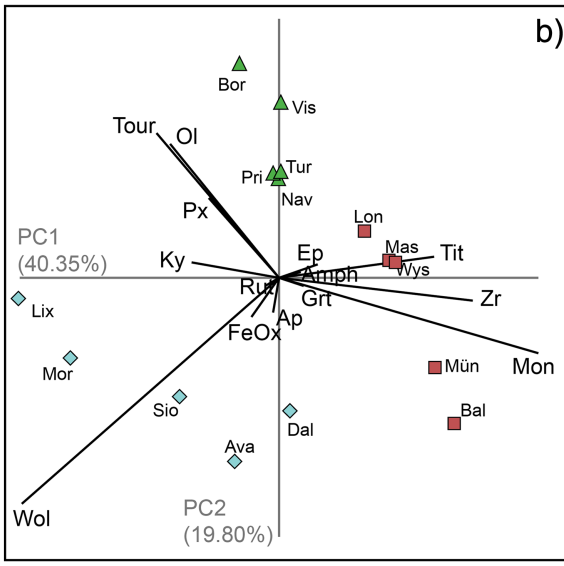
b)
Bor
Vis
Tour
Ol
Pri
Tur
Nav
Px
Lon
PC1
(40.35%)
Ky
Ep
Mas
Tit
Amph
Wys
Rut
Grt
Zr
Lix
Ap
FeOx
Mor
Mün
Mon
Sio
Dal
Bal
Ava
Wol
PC2
(19.80%)

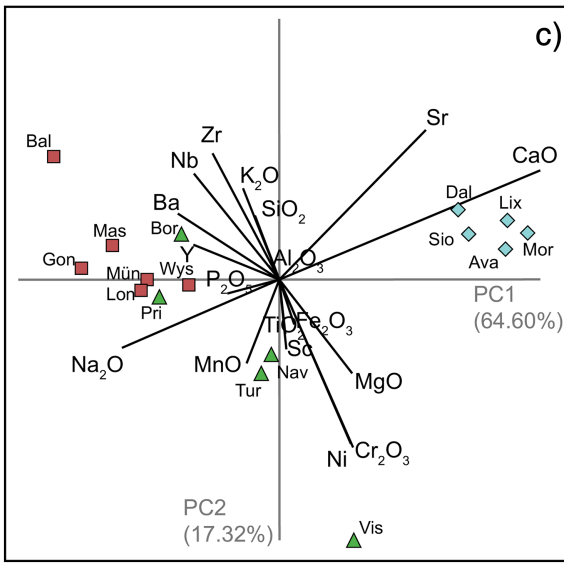
c)
Sr
Bal
Zr
CaO
Nb
K_2O
Dal
Ba
SiO_2
Lix
Bor
Mas
Sio
Mor
Y
Gon
Al_2O_3
Ava
Mün
Wys
P_2O_5
Lon
PC1
(64.60%)
Pri
TiO_2
Fe_2O_3
Sc
Na_2O
MnO
Nav
MgO
Tur
Ni
Cr_2O_3
PC2
(17.32%)
Vis

Figure 2

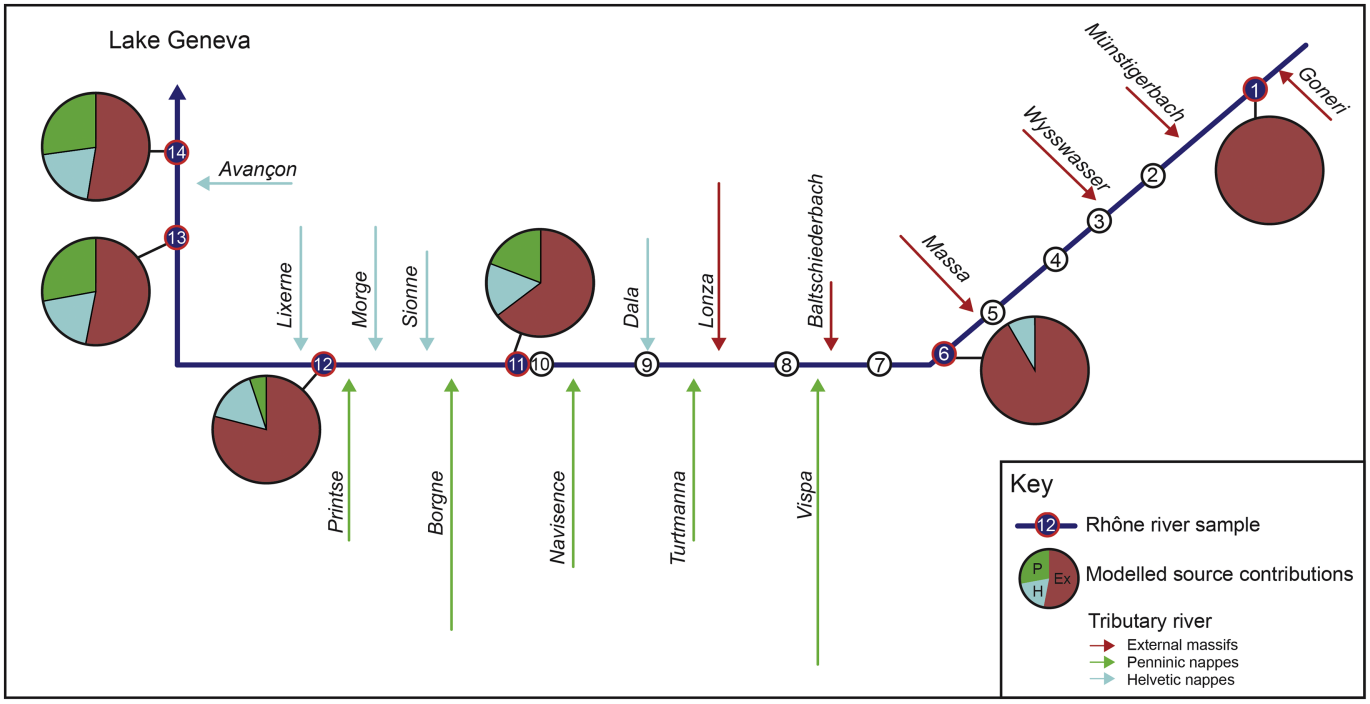
Lake Geneva
Avançon
Lixerne
Morge
Sionne
Dala
Lonza
Baltschiederbach
Massa
Wysswasser
Münstigerbach
Goneri
Printse
Borgne
Navisence
Turtmanna
Vispa
1
2
3
4
5
6
7
8
9
10
11
12
13
14
Key
Rhône river sample
P
Ex
H
Modelled source contributions
Tributary river
External massifs
Penninic nappes
Helvetic nappes

Figure 3

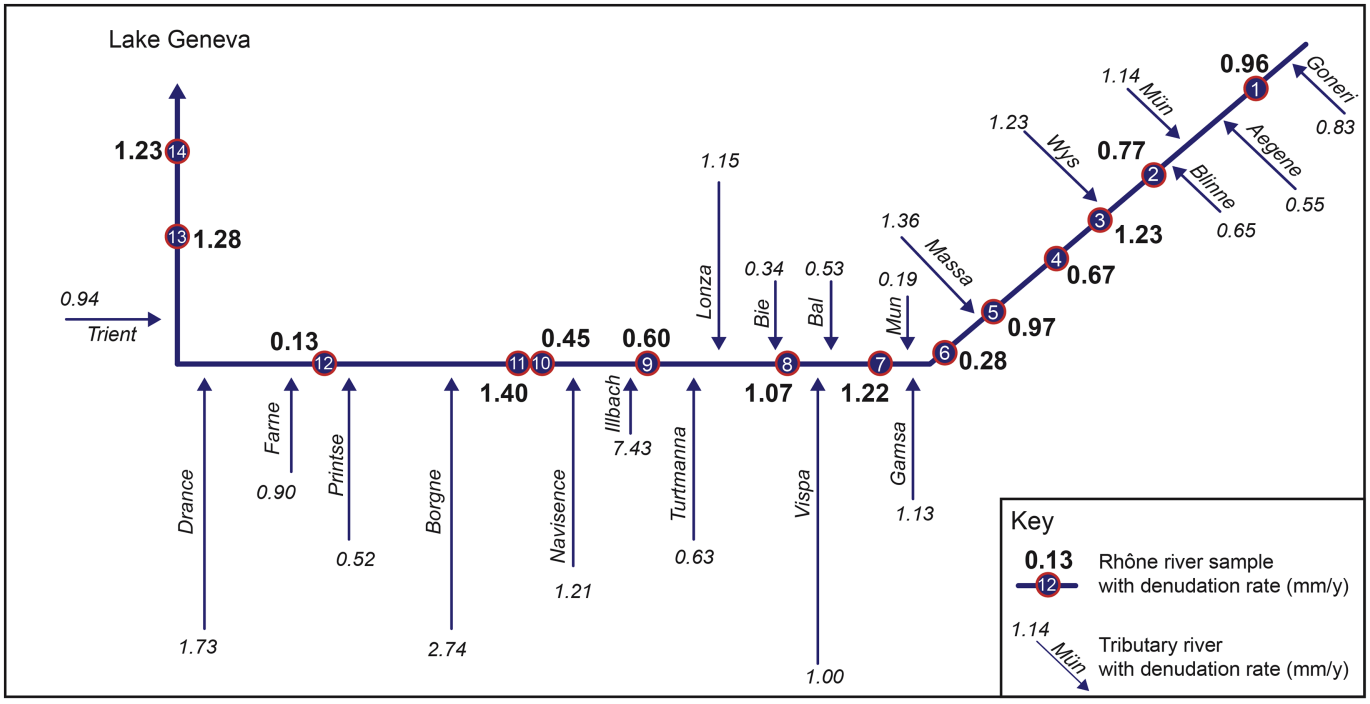
Lake Geneva
1.23
14
13
1.28
0.94
Trient
0.13
12
11
10
0.45
0.60
9
1.40
8
1.07
7
1.22
6
0.28
5
0.97
4
0.67
3
1.23
2
0.77
1
0.96
1.15
Lonza
0.34
Bie
0.53
Bal
0.19
Mun
1.36
Massa
1.23
Wys
1.14
Miin
Goneri
0.83
Aegene
0.55
Blinne
0.65
Drance
1.73
Farne
0.90
Printse
0.52
Borgne
2.74
Navisence
1.21
Illbach
7.43
Turtmanna
0.63
Vispa
1.00
Gamsa
1.13
Key
0.13
12
Rhône river sample with denudation rate (mm/y)
1.14
Miin
Tributary river with denudation rate (mm/y)

Figure 4

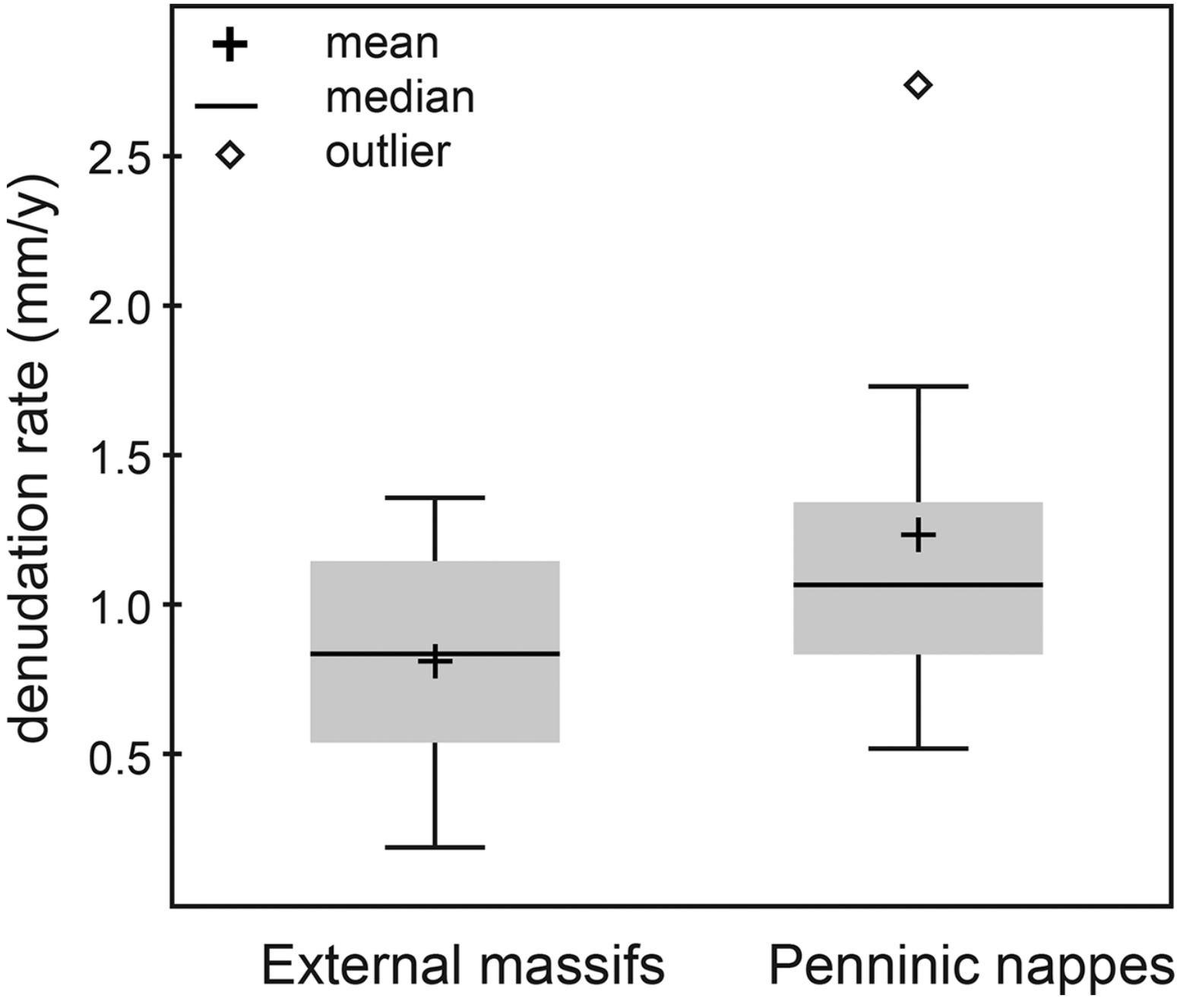
mean
median
outlier
2.5
2.0
1.5
1.0
0.5
denudation rate (mm/y)
External massifs
Penninic nappes

Figure 5

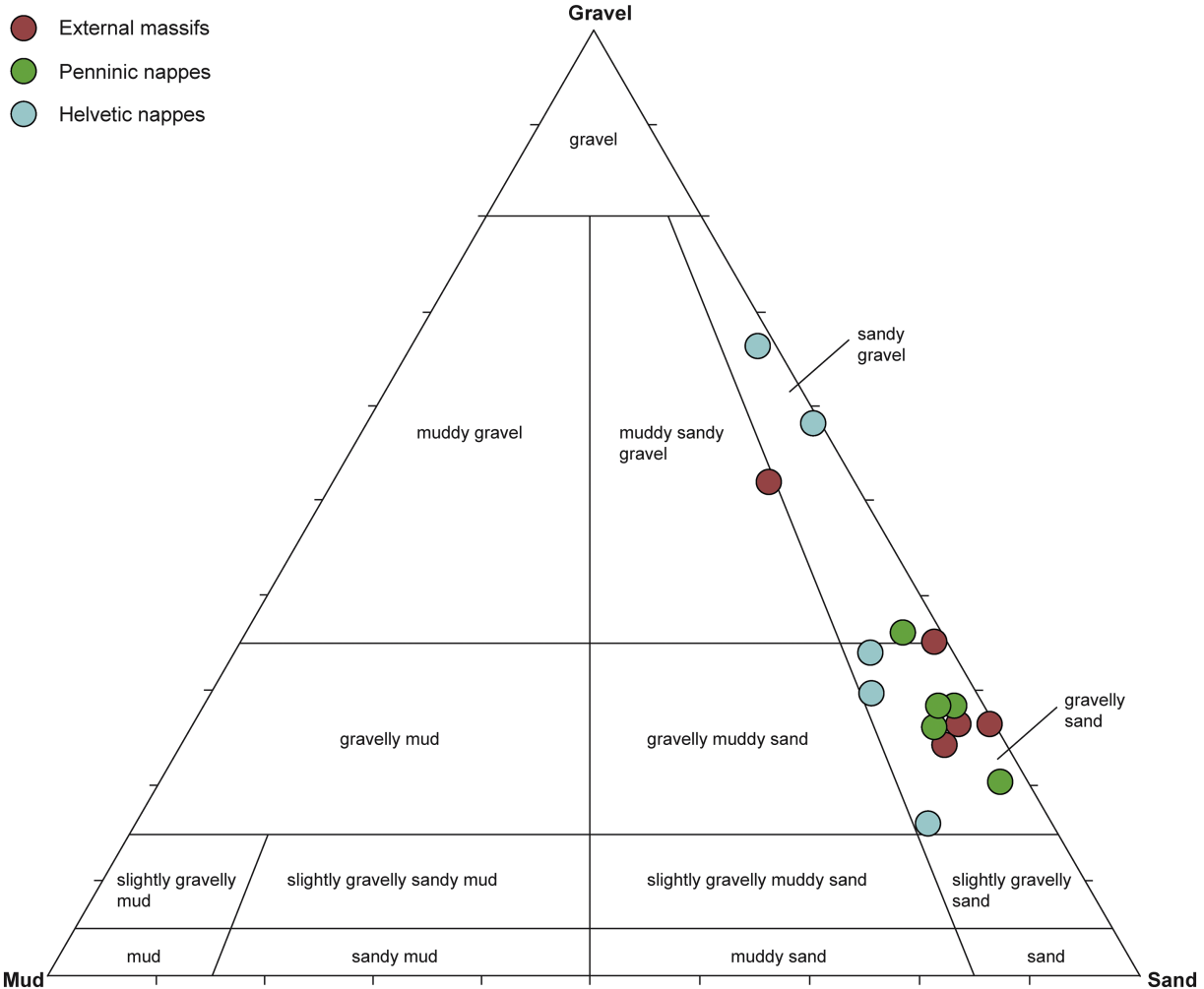
External massifs
Penninic nappes
Helvetic nappes
Gravel
gravel
sandy gravel
muddy gravel
muddy sandy gravel
gravelly mud
gravelly muddy sand
gravelly sand
slightly gravelly mud
slightly gravelly sandy mud
slightly gravelly muddy sand
slightly gravelly sand
mud
sandy mud
muddy sand
sand
Mud
Sand

Figure 6

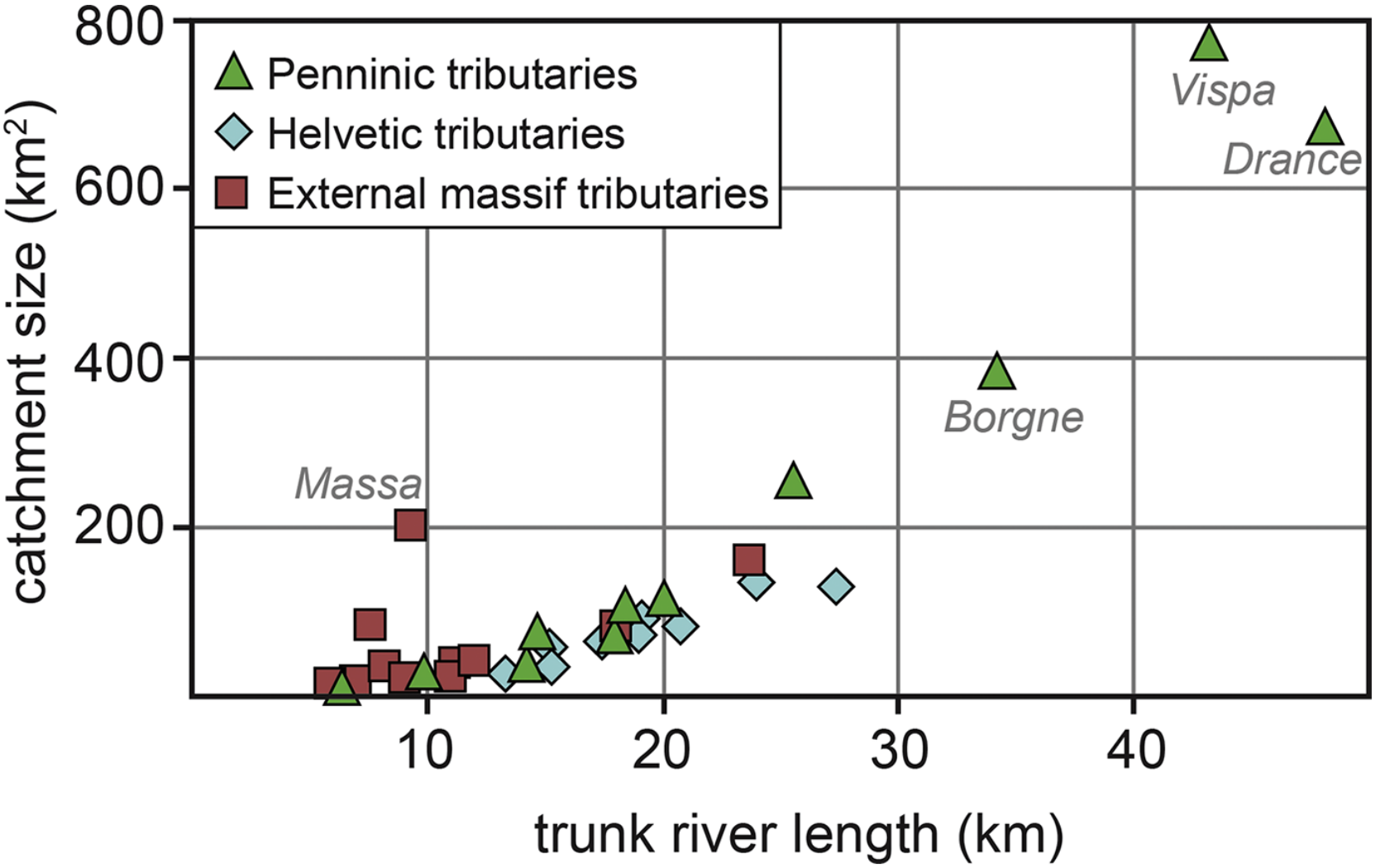
Penninic tributaries
Helvetic tributaries
External massif tributaries
Vispa
Drance
Borgne
Massa
800
600
400
200
10
20
30
40
catchment size (km²)
trunk river length (km)

Figure 7

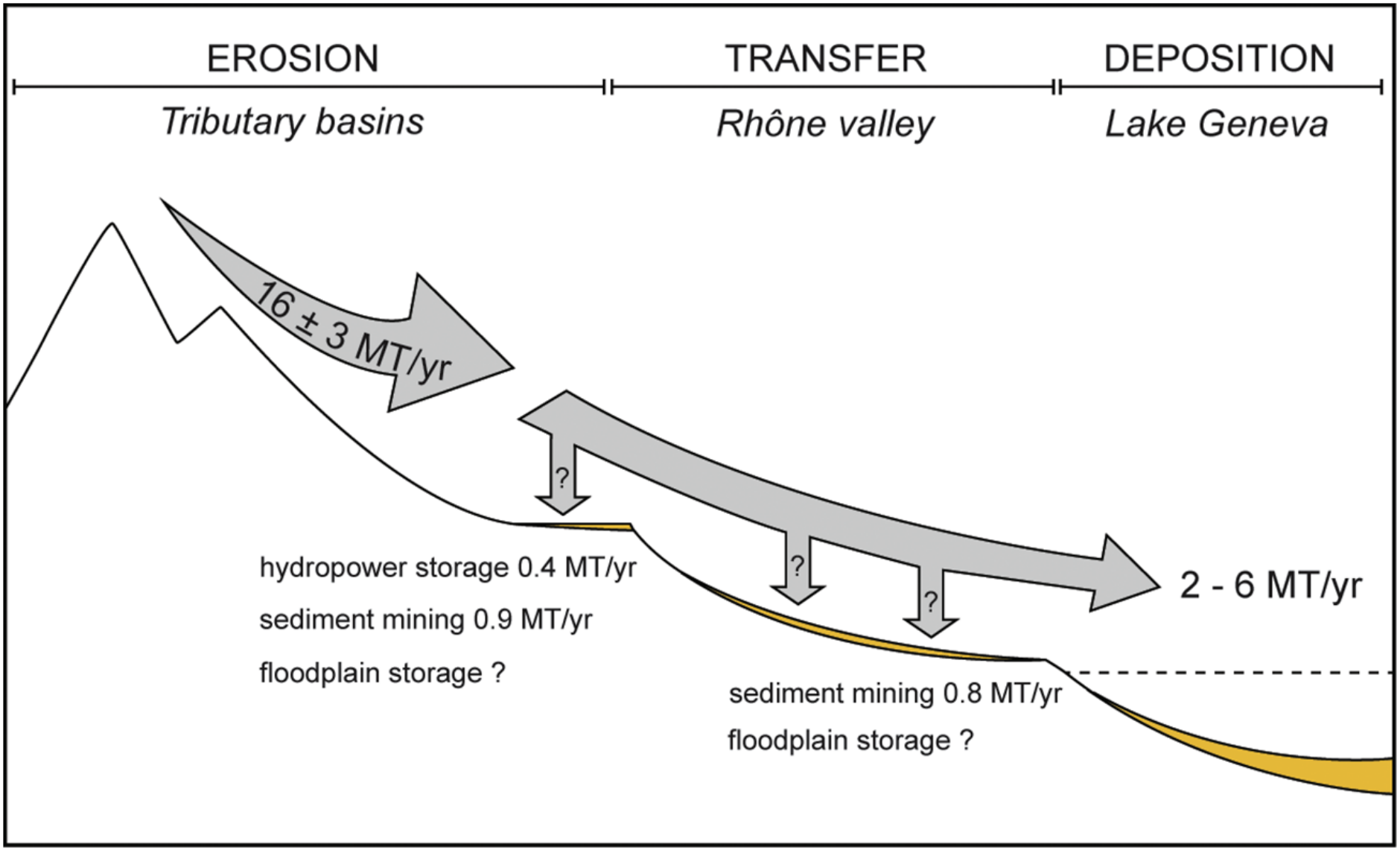
EROSION
TRANSFER
DEPOSITION
Tributary basins
Rhône valley
Lake Geneva
16 ± 3 MT/yr
?
?
?
hydropower storage 0.4 MT/yr
sediment mining 0.9 MT/yr
floodplain storage ?
2 - 6 MT/yr
sediment mining 0.8 MT/yr
floodplain storage ?

Figure 8